UCRL 10252

University of California

Ernest O. Lawrence Radiation Laboratory

TWO-WEEK LOAN COPY

This is a Library Circulating Copy which may be borrowed for two weeks. For a personal retention copy, call Tech. Info. Division, Ext. 5545

SCATTERING OF NEGATIVE PIONS ON PROTONS AT 310 MeV: DIFFERENTIAL AND TOTAL CROSS-SECTION AND PHASE-SHIFT ANALYSIS

Berkeley, California

DISCLAIMER

This document was prepared as an account of work sponsored by the United States Government. While this document is believed to contain correct information, neither the United States Government nor any agency thereof, nor the Regents of the University of California, nor any of their employees, makes any warranty, express or implied, or assumes any legal responsibility for the accuracy, completeness, or usefulness of any information, apparatus, product, or process disclosed, or represents that its use would not infringe privately owned rights. Reference herein to any specific commercial product, process, or service by its trade name, trademark, manufacturer, or otherwise, does not necessarily constitute or imply its endorsement, recommendation, or favoring by the United States Government or any agency thereof, or the Regents of the University of California. The views and opinions of authors expressed herein do not necessarily state or reflect those of the United States Government or any agency thereof or the Regents of the University of California.

Research and Development

UCRL-10252

UC-34 Physics
TID-4500 (17th Ed.)

UNIVERSITY OF CALIFORNIA

Lawrence Radiation Laboratory
Berkeley, California

Contract No. W-7405-eng-48

SCATTERING OF NEGATIVE PIONS ON PROTONS AT 310 MeV: DIFFERENTIAL AND TOTAL CROSS-SECTION AND PHASE-SHIFT ANALYSIS

Hugo R. Rugge

(Ph. D. Thesis)

May 20, 1962

Printed in USA. Price $2.00. Available from the
Office of Technical Services
U. S. Department of Commerce
Washington 25, D.C.

SCATTERING OF NEGATIVE PIONS ON PROTONS AT 310 MeV: DIFFERENTIAL AND TOTAL CROSS-SECTION AND PHASE-SHIFT ANALYSIS

Contents

Abstract v

I. Introduction 1

II. DCS Experimental Method

A. Experimental Arrangement 5

1. Magnet System 5

2. Pion Beam 7

3. Counters 10

4. Electronics 13

5. Liquid Hydrogen Target 13

B. Counter Telescope 15

1. Design 15

2. Telescope Calibration at Forward Angles 15

C. Experimental Procedure 17

1. Accidentals and Background 17

2. Cross-Section Measurement 19

3. Simultaneous Experiment 21

D. Normalization Measurement 21

1. Experimental Arrangement 22

2. Experimental Procedure 22

III. DCS Results

A. Corrections to Data 26

1. Electron Contamination in the Scattered Pion Beam . 26

2. Counter Telescope Efficiency 33

3. Finite Target and Telescope 35

4. Other Corrections 35

B. Normalization Corrections 36

Contents (continued)

C. Differential Cross Section 37
1. Scattered Pions Counted 37
2. Target Constant 37
3. Normalization 39
D. Errors 43
IV. Total Cross Section
A. Experimental Method 45
1. Experimental Arrangement 45
2. Experimental Procedure 47
B. Results and Errors 47
V. Phase-Shift Analysis
A. Relationship of Phase Shifts to Experimental Data . . . 51
1. Scattering Amplitudes 51
2. Isotopic Spin 53
3. Notation 53
B. Search Program 55
1. General Method 55
2. PIPANAL 1CF4 56
C. Phase-Shift Investigations 58
1. spd Investigations 64
2. spdf Investigations 67
3. Inelastic Scattering 69
VI. Discussion of Results 70
Acknowledgments 73
Appendices
A. Inclusion of Coulomb Scattering in Pion-Nucleon Scattering Amplitudes 74
B. Tables of Error Matrices for spd and spdf Solutions. . . 79
References 84

SCATTERING OF NEGATIVE PIONS ON PROTONS AT 310 MeV: DIFFERENTIAL AND TOTAL CROSS-SECTION AND PHASE-SHIFT ANALYSIS

Hugo R. Rugge

Lawrence Radiation Laboratory
University of California
Berkeley, California

May 20, 1962

ABSTRACT

The differential cross section in π^--p elastic scattering at 310-MeV incident-pion energy has been measured for 28 angles in the laboratory system angular region 25 deg $\leq \theta_{lab} \leq$ 160 deg. The reaction was observed by counting the scattered pions emerging from a liquid hydrogen target with a counter telescope consisting of scintillation and Cerenkov counters. A measurement of the total cross section by attenuation as a function of cutoff angle was also performed, using scintillation counters. These data were incorporated with polarization and other differential cross section data at this energy, and a phase shift analysis was performed. An IBM 7090 search program was developed for this purpose.

Analysis of all data for spd waves (up to $\ell = 2$) has resulted in a single acceptable solution that has I-spin 3/2 phase shifts in excellent agreement with results of a previous π^+-p phase shift analysis, and has I-spin 1/2 phase shifts that are < 6 deg for the $D^{5/2}$ shift which is ≈ 15 deg. Errors on the phase shifts vary from 0.4 through 1.1 deg.

An extension of the analysis to spdf waves (up to $\ell = 3$) results in two probable solutions, and one that is rather unlikely. These, as well as the spd solution, are discussed. Errors on the spdf solution are larger, ranging up to 2 deg.

I. INTRODUCTION

The interaction of pions and nucleons is of fundamental importance in nuclear physics because of the relationship of this pion-nucleon interaction to nuclear forces. It is at present believed that nuclear forces result principally from an interchange of pions by the nucleons in the nucleus. For this reason, the pion-nucleon interaction has been studied for some time, for the most part by measuring differential and total cross sections for the scattering of positive and negative pions on protons. Although there is a reasonable amount of data, most of it lacks completeness and accuracy at any single energy. Therefore, it was our purpose to obtain accurate and complete π^--p differential and total cross-section data at one energy, 310 MeV. (In this report, energies mentioned refer to incident-pion kinetic energies.)

This work was part of a continuing effort at the Lawrence Radiation Laboratory to obtain accurate data concerning the pion-nucleon interaction at 310 MeV. Previously, Rogers et al. had made accurate measurements of 25 differential cross section points for the reaction

$$\pi^+ + p \rightarrow \pi^+ + p,^{1} \tag{1.1}$$

and Foote et al. had obtained recoil proton polarization data at four angles for this same interaction.[2] These constituted the most accurate and complete data on π^+-p scattering ever obtained at one energy. However, investigation of π^+-p scattering leads only to information about the isotopic spin 3/2 state of the pion-nucleon system. To gain information about the I-spin 1/2 state either of the two following π^--p interactions must be studied:

$$\pi^- + p \rightarrow \pi^- + p \qquad \text{(elastic scattering)}, \tag{1.2}$$

or

$$\pi^- + p \rightarrow \pi^0 + n \qquad \text{(charge-exchange scattering)}. \tag{1.3}$$

Because the detection of charged particles is considerably easier than the detection of neutrals, we proposed to study Reaction (1.2), the elastic scattering of pions on protons. It was our aim to obtain information about this interaction at least as accurate as the π^+-p data previously obtained by Rogers et al.[1]

The main reason for lack of accuracy in previous measurements was that only low-intensity pion beams were available to experimenters. These low intensities resulted in low counting rates which, of course, led to poor counting statistics and to limitations on the number of angles at which data could be obtained. Furthermore, when counting rates are low there is no opportunity to investigate possible systematic errors thoroughly.

We were able to form a pion beam that contained 3×10^6 π^-/sec in a 2-in.-diam circle or a flux of about $1.5\times10^5 \pi^-/\text{cm}^2$-sec. This was about two orders of magnitude better than had been obtained by most previous experimenters. By scattering this beam from a liquid hydrogen target and detecting the scattered pions with counters, we were able to measure 28 differential cross-section points as a function of laboratory-system (lab) angle and to obtain total cross-section data.

One of the chief purposes of obtaining experimental data is to be able to use it either to check theoretical predictions or to indicate the correct theoretical approach. The usual meeting place of theory and experiment for elastic scattering has been at the phase shifts. Data obtained from pion-nucleon scattering experiments are usually analyzed in terms of partial waves. In this type of analysis, scattering amplitudes are expanded in a series of terms, each term corresponding to a definite angular momentum state of the pion-nucleon system. States with the orbital-angular momentum quantum number $\ell = 0, 1, 2, 3 \cdots$ are referred to as s, p, d, f $\cdots$ states. These partial-wave expansions contain parameters, called phase shifts, that measure the magnitude of the interaction in any given angular momentum and I-spin state, and it is the value and energy dependence of these phase shifts that a theory must predict to be successful.

For this reason, a search for the phase shifts describing the pion-nucleon interaction at 310 MeV was initiated. Such an analysis had already been completed by Foote for the π^+-p data,[3] yielding I-spin 3/2 phase shifts. We have extended this work, using all of the π^+ data, the data contained in this report, and the recoil-proton polarization data measured by Vik.[4] In addition, charge-exchange differential cross-section data at 317 MeV measured by Caris was also used.[5] Some π^--p differential cross-section and polarization data at 307 MeV had been previously measured by Zinov and Korenchenko,[6] and Vasilevskii and Vishnyako,[7] but these data were insufficiently accurate for good phase-shift analysis.

One reason for the original choice of an incident pion energy of 310 MeV was that classically, d waves are expected to become noticeable in the interaction at about 300 MeV. The results of an spd (up to $\ell = 2$) phase-shift analysis led to rather large d waves and, therefore, the analysis was extended to include f waves.

Results and descriptions of the spd and spdf phase-shift analysis, as well as details and results of the differential and total cross-section measurements, are contained in this report.

For convenience, throughout this report we refer to the differential and the total cross section as DCS and TCS, respectively.

II. DCS EXPERIMENTAL METHOD

A. Experimental Arrangement

In order to achieve the degree of accuracy desired for the DCS measurement, an intense 310-MeV π^- beam had to be produced and scattered from liquid hydrogen. The desired pion beam was produced and was focused on a liquid hydrogen target by a magnet system. For most of the experiment the pion beam striking the hydrogen target was monitored by an argon-filled ionization chamber. The pions scattered by the liquid hydrogen were detected by a counter telescope consisting of a Cerenkov counter and two scintillation counters. During part of the experiment, the incident pion beam was monitored by a pair of scintillation counters to obtain a more accurate normalization of the DCS. The DCS was measured at a total of 28 lab angles.

A diagram of the experimental arrangement is shown in Fig. 1.

1. Magnet System

Negative π mesons were produced by inserting a beryllium target into the 740-MeV internal proton beam of the Berkeley 184 inch synchrocyclotron. The pions produced at 0 deg were deflected out of the cyclotron by its own magnetic field, and passed through a thin aluminum window in the vacuum tank and into the 8 in. aperture of the two-section (doublet) quadrupole magnet Q_1. This quadrupole formed a parallel beam that passed into an 8-ft-long iron collimator known as the Meson Wheel. From the Wheel the beam entered the experimental area known as the Meson Cave, where it then impinged upon another focusing quadrupole magnet Q_2. This magnet also had an 8 in. aperture and two sections. Upon leaving Q_2 the beam was momentum-analyzed by a bending magnet M_1. The angle of deflection chosen was 36 deg, to compensate for the momentum dispersion in the pion beam introduced by the cyclotron field. The combined effect of Q_2 and M_1 was to focus an image of the pion source on the liquid hydrogen target.

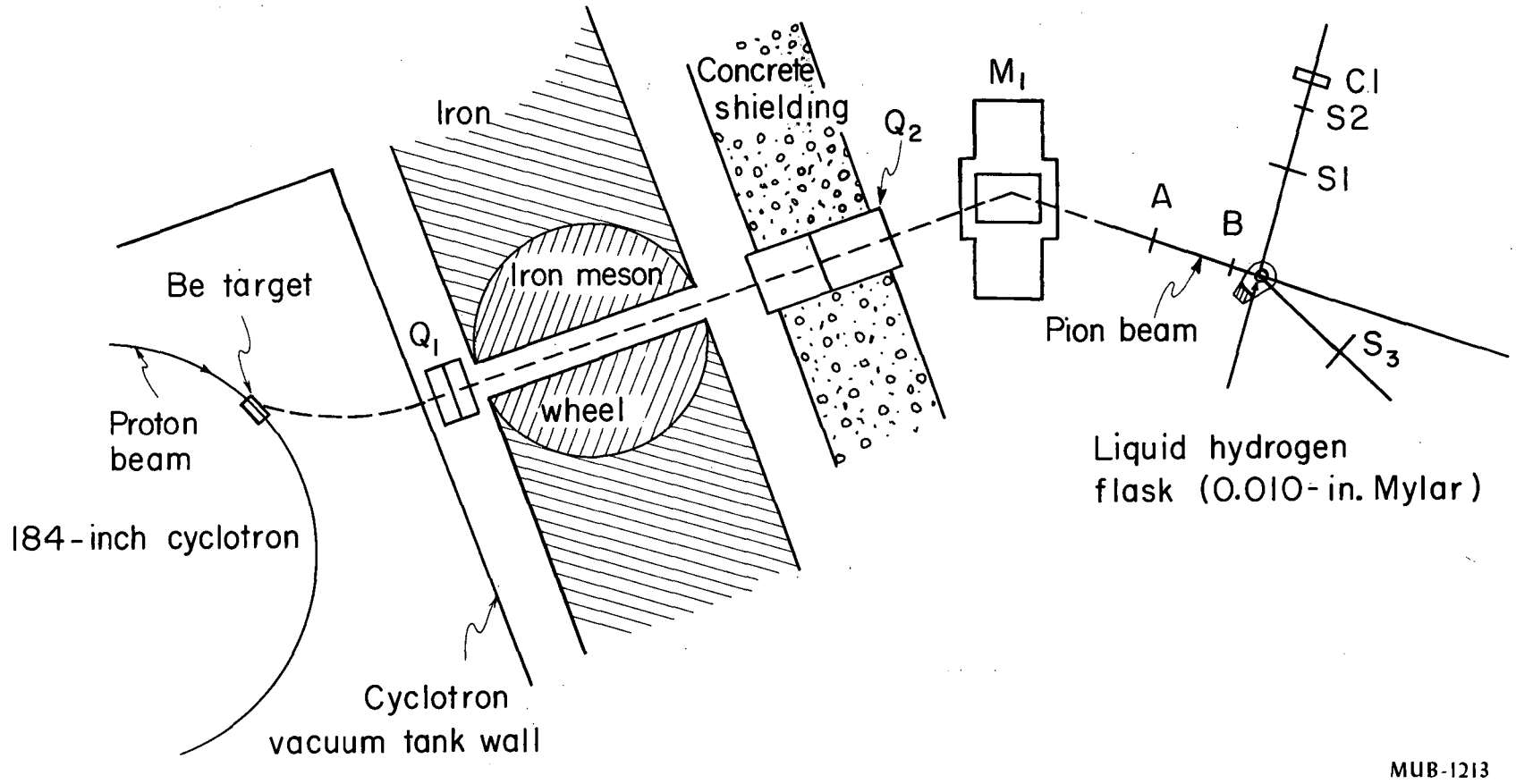

Fig. 1. Diagram of experimental arrangement for DCS measurement.

Current settings for the quadrupole magnets were calculated by an IBM 650 program called DIPOLE. The current in the bending magnet M_1 was accurately determined by the suspended-wire technique, which was also used to check the currents in Q_2. Fine tuning of the focusing magnets was done with the pion beam and the beam profile counters described below.

After leaving the magnet system and before striking the hydrogen target, the pion beam passed through a 10 in.-long brass collimator surrounded by lead. This collimator was designed to attenuate the spatial components of the pion beam which were directed toward the heavy aluminum flanges supporting the liquid hydrogen target (see Fig. 2). These components were the main source of coincidence counts when the hydrogen flask was empty. The collimator was used only when the incident beam was monitored by the ionization chamber.

2. Pion Beam

The internal beryllium target used to produce the pions lay 2 in. along the beam direction. Its position in the cyclotron was determined experimentally to give the maximum-intensity π^- beam at the position of the liquid hydrogen target. The intensity measurements were made with a 7 in.-diam argon-filled ionization chamber.[8] Because of the sensitivity of the beam intensity and its position at the hydrogen target on the radial position of the beryllium target, it was necessary to experimentally realign the internal target daily. The correct alignment of the internal target was verified with the beam profile counters.

A check of the energy spread of the pion beam at the hydrogen target was made by taking an integral range curve of the beam in copper (see Fig. 3). A determination of the muon contamination of the beam was also made from this range curve.

Horizontal and vertical beam profiles were made at the hydrogen target position, using two square plastic scintillators (0.25 in. and 0.50 in. on a side, respectively) in coincidence. These profiles were taken with and without the brass collimator in position (see Fig. 2). The beam channel through the magnet system was enclosed by plastic bags filled with helium, whose purpose was to reduce the multiple Coulomb scattering of the pion beam which would increase the size of the beam at the liquid hydrogen target.

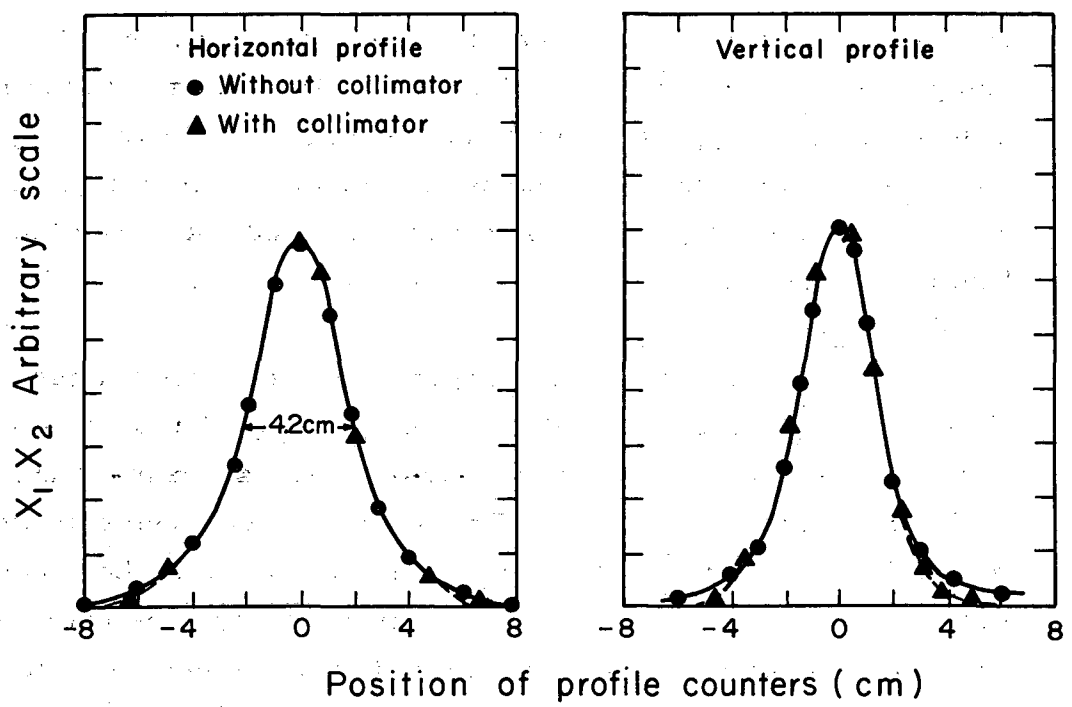

MU-27131

Fig. 2. Horizontal and vertical beam profiles, taken at the position of the liquid hydrogen target with and without the brass collimator.

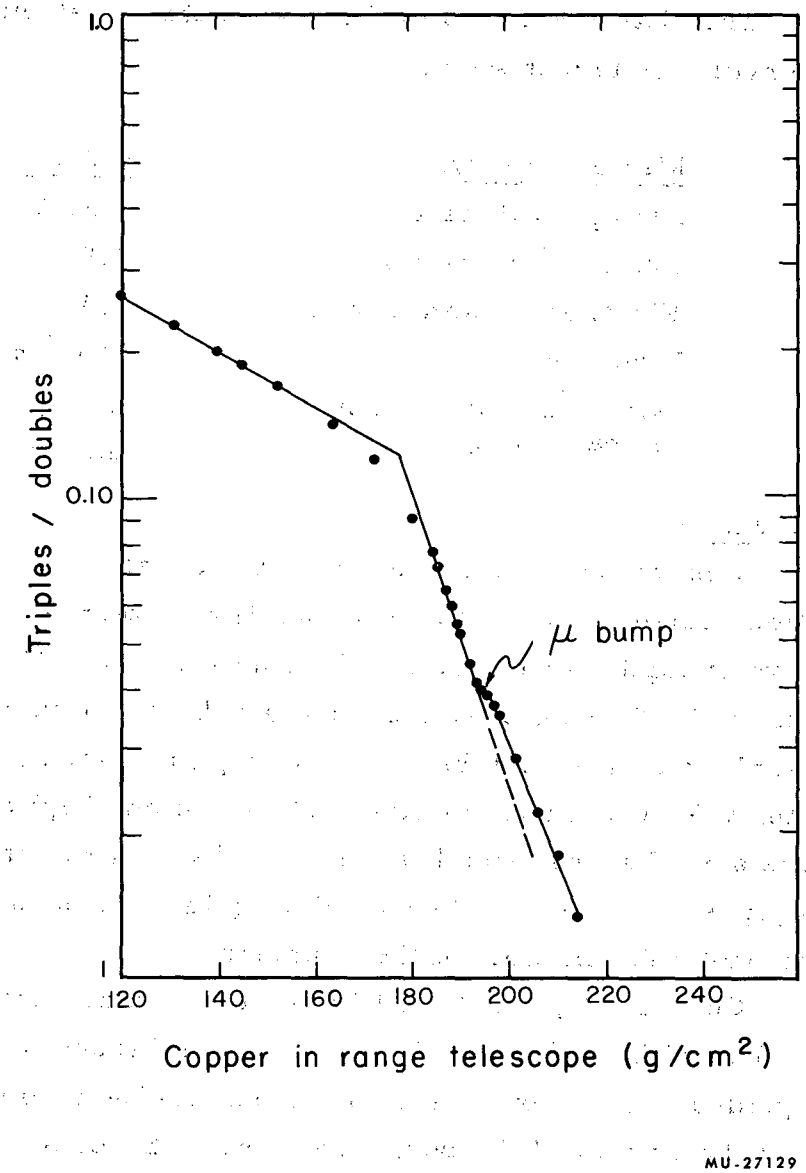

Fig. 3. Integral range curve of incident pion in copper.

The electron contamination of the beam was measured by using a gas Cerenkov counter filled with sulfur hexafluoride[9] (see Sec. III. B. 1).

The characteristics of the beam obtained at the position of the liquid hydrogen target were:

Median energy:	310 ± 3 MeV
Energy half-width	5 MeV
Total μ^- contamination	4.5%
Electron contamination	0.3%
Intensity	$3\times10^6\ \pi^-$/sec
Beam size (full width at half-max)	3.2 cm vertical × 4.2 cm horizontal

3. Counters

Most of the counters used in this experiment were plastic scintillation counters made of a solid solution of terphenyl in polystyrene. The two exceptions were liquid Cerenkov counter C1, and a gas Cerenkov counter CG. The light from almost all the counters was viewed with RCA 6810A photomultiplier tubes. The exceptions were the gas Cerenkov counter CG, which used an RCA 7232A photomultiplier, and the beam-profile scintillators, which were viewed with 1P21 phototubes. Lucite light pipes or aluminum (Alzak) light guides were used to guide the light to the phototube on most of the counters.

Counter C1, the liquid Cerenkov counter, consisted of a rectangular box with 1/16 in. lucite walls. The Cerenkov light from the liquid was guided to the phototube by a cylindrical lucite light pipe fitted into a hole at the bottom of the box. Water was chosen as the Cerenkov radiator to give a β (= v/c) threshold of 0.75. This threshold allows the counter to reject all recoil protons and most inelastic pions from the liquid hydrogen target.

Data concerning all the counters used in this experiment are found in Table I.

The positions of the counters used in the DCS measurement are shown in Fig. 4. Not all the counters shown were used in all phases of the DCS measurement.

Table I. Description of counters used in DCS and TCS measurements.

Counter number	Type	Light guide or pipe	Size	Thickness (in.)
A	Plastic scint.	Alum.	4 in. diam	1/8
B	Plastic scint.	Alum.	3 in. diam	1/16
S1	Plastic scint.	Alum.	4 in. diam	1/16
S2	Plastic scint.	Lucite	2-1/4in. diam	1/4
S3	Plastic scint.	Lucite	12×12 in.	3/4
C1	H_2O Cerenkov	Lucite	4×4 in.	1-1/2
S4	Plastic scint.	Alum.	3 in. diam	1/8
S5	Plastic scint.	Alum.	1-1/2 in. diam	1/16
S6	Plastic scint.	Lucite	10 in. diam	3/4
X1	Plastic scint.	-	1/4×1/4 in.	3/8
X2	Plastic scint.	-	1/2×1/2 in.	3/8
CG	SF_6 gas Cerenkov	Alum.	6 in. diam	48

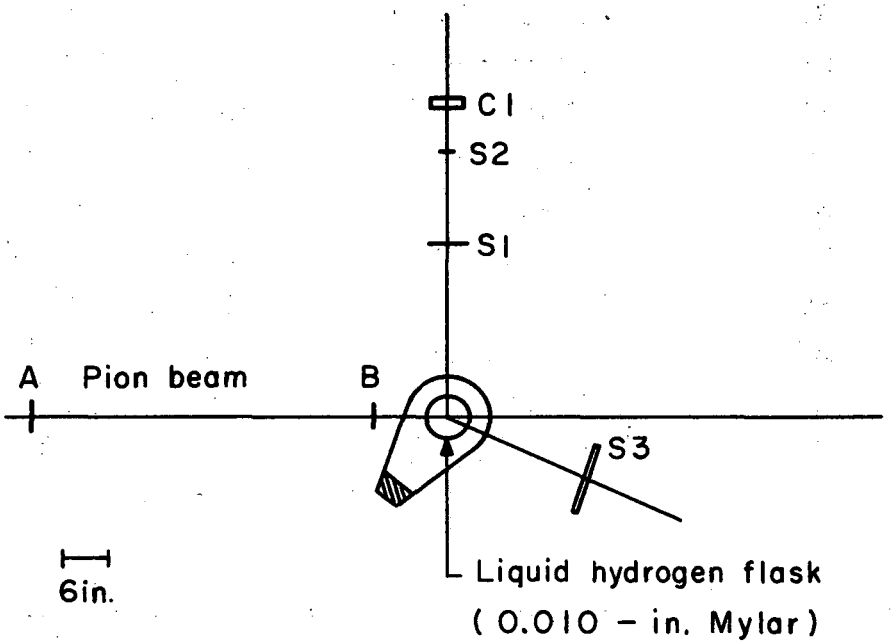

MU-27132

Fig. 4. Diagram of liquid hydrogen target and counter arrangement.

4. Electronics

A schematic diagram of the electronics used with DCS measurement is shown in Fig. 5. The pulses from the photomultipliers were delayed with respect to one another, by use of RG-63/U cable in delay boxes. Counters S1 and C1 were amplified by Hewlett-Packard 460A wideband amplifiers. The properly delayed pulses from all the counters were fed into a multi-input coincidence circuit of the Garwin type.[10] The output pulses of the coincidence circuit were fed into 10 Mc discriminating units[11] that in turn drove conventional scaling units. The resolving time of the system was approx 20×10^{-9} sec. The appropriate counter voltages and delays were determined experimentally by optimizing the coincidence rate with respect to these variables. This was done in the incident pion beam at low intensity. These settings were checked at a number of different scattering angles during the experiment.

The ion-chamber current was transmitted to a standard integrating electrometer by double-shielded cable, and displayed on a recorder.

A scaler-gater unit was used to turn the ion-chamber electrometer and all scaling units on or off simultaneously.

5. Liquid Hydrogen Target

The liquid hydrogen target consisted of an upright cylinder 6 in. in diameter and 8 in. high, made of 0.010 in. Mylar. This flask was surrounded by a vacuum, and a 270 deg window of 0.030 in. Mylar 6 in. high was centered vertically on the flask. This window was supported by heavy aluminum flanges to meet hydrogen safety requirements.

Above the flask was a hydrogen reservoir surrounded by a liquid nitrogen jacket.

During the experiment the flask was emptied of liquid hydrogen to obtain background measurements by closing a flask vent value that ordinarily allowed the hydrogen gas to escape into the atmosphere. With the value closed, the hydrogen gas pressure forced the liquid hydrogen out of the flask and up into the reservoir. The target was refilled by opening the vent value.

At three of these energies integral range curves were taken of the incident beam, both to check its energy and to determine the muon contamination of the beam. Values of muon contaminations at other energies were interpolated from a curve of the three points obtained by the range curve.

The greatest amount of copper used in the telescope was 33.6 g/cm^2 at 25 deg laboratory angle. This corresponded to an attenuation of about 20%. A list of the amount of copper used at each angle, and the calculated efficiency at that angle, is given in Table II.

Measurements of the scattering out of pions by counter S2 and the efficiency of the Cerenkov counter (C1) was also obtained at this time by recording the S1, S2 C1/S1, S2 ratio, with no copper in the counter telescope.

Table II. Forward angle counter telescope efficiencies.

θ_{lab} (deg)	Efficiency	Amount Cu in telescope (g/cm^2)
25	0.802	33.6
30	0.850	25.5
35	0.867	22.6
40	0.890	16.7
45	0.918	13.9
50	0.955	8.6
55	0.967	5.4
60	0.976	3.7
65	0.978	3.3
70	1.00	0.0

C. Experimental Procedure

1. Accidentals and Background

Accidentals in the counter telescope were measured in the usual manner. Each counter in the telescope was delayed in turn, with respect to the remaining counters, by 54×10^{-9} sec (the time difference between two successive cyclotron rf pulses). The accidental coincidence rate of the telescope was found to be < 0.1% of the true counting rate at all angles, and hence negligible.

The most important source of background comes from the scattering of pions in the walls of the hydrogen-containing flask and surrounding material. This background can be measured by emptying the flask of hydrogen and measuring the target-empty rate. This rate varied over different scattering angles from approx 25 to 50% of the target-full rate.

A more difficult form of background to measure is a contamination by electrons (the term electrons is used throughout this paper to mean both positrons and negative electrons unless otherwise noted) in the scattered pion beam. These electrons result because the production of neutral pions in the charge-exchange reaction (2.1) takes place in the liquid hydrogen. The subsequent decay of the π^0 produces the electrons

$$\pi^- + p \rightarrow \pi^0 + n; \tag{2.1}$$

$$\pi^0 \rightarrow \gamma + \gamma, \tag{2.2}$$

or

$$\pi^0 \rightarrow \gamma + e^+ + e^-. \tag{2.3}$$

The electron background arises from the two decay modes of the π^0 indicated above (2.2, 2.3). In the first (2.2), the two gammas may interact with the hydrogen and surrounding materials to produce electron-positron pairs. The counter telescope cannot distinguish between an electron and an elastically scattered pion. In the second decay mode (2.3), the $e^+ + e^-$ pair is produced directly in the π^0 decay (Dalitz pair).[12]

A detailed discussion of the magnitude of this background as a function of scattering angle is found in Sec. III. A. 1.

It was possible to make some experimental checks on the calculations of electron contamination described in Sec. III. A. 1. These are described below.

The first source of background is due to the conversion of γ rays in the target and surrounding material, and is therefore proportional to the amount of material between the scattering point and the counter telescope. Approximately 1% of the γ's coming from the target are converted into pairs by this material.

The calculations on contamination were checked by increasing the amount of converting material between the target and counter telescope. From one to five 0.15-g/cm^2 sheets of Cu were placed next to the target, and the counting rates in the counter telescope obtained for each case with the liquid hydrogen target both full and empty. Each of these copper sheets converted roughly the same number of γ's from the charge-exchange reaction as did the target without copper.

The "effective target thickness" of the copper as a function of scattering angle was computed by IBM 704 program ALPHA BAR. The data points with copper, as well as one without, obtained by subtracting target-empty from target-full data, were then plotted against effective target thickness, and a least-squares fit of a straight line was made. The difference in rates between "zero target thickness" and "one target thickness" gave the conversion-electron contamination. A total of six angles were checked in this way. Because this effect is relatively small, the uncertainty in measured values of this background owing to counting statistics is believed larger than that obtainable from a careful calculation of this effect. This calculation as made is described in Section III. A. 1. It gives an electron contamination for the elastically scattered pion beam of about 5% at most angles.

Values obtained from the measurements are in statistical agreement with the calculation.

The second source of background is the Dalitz pairs. A calculation method for this contamination is also discussed in Sec. III. A. 1. No direct measurement of the contamination was made, but a check on the total background due to charge-exchange scattering can be obtained by putting a

conjugate counter in coincidence with the counter telescope. This counter (S3) was placed at an appropriate angle on the other side of the target to record the proton conjugate to the elastically scattered pions counted in the counter telescope. Essentially, none of the electrons can duplicate this coincidence between the conjugate counter and counter telescope; hence, a comparison of rates with and without the conjugate counter in coincidence can give the contamination at those angles where such a measurement can be made.

Unfortunately, the angles at which the measurements can be made (approximately 90 to 100 deg pion lab scattering angle) are severely limited by two considerations. If the conjugate proton counter is moved closer to zero deg (larger pion scattering angles) it will intercept the incident pion beam and be jammed by it. If, on the other hand, the conjugate counter is moved to larger angles (forward pion scattering angles) the protons will have barely enough energy to get out of the target, and if they do, they will be badly multiply scattered. Even at the angles measured (90 and 100 deg lab pion scattering angle) the correction that must be made for the multiple scattering of the protons introduced in the value of the cross section an uncertainty larger than the statistical counting error of about 2%. For this reason, this method serves only as a rough check on the total electron background. The values obtained above are in agreement with the calculation described in Sec. III. A. 1.

The calculated values of the electron contamination corrections as a function of scattering angle are given in Table III.

2. Cross-Section Measurement

Data for the cross-section measurement were taken at 28 lab scattering angles from 25 to 160 deg in 5-deg steps, and were taken in cycles of hydrogen target full and empty. Generally speaking, several such cycles were observed and then the counter telescope was moved to a different angle.

The counting rates with the target full varied from approximately 30 counts/sec at the forward pion scattering angles to approximately 1 count/sec in the background angular region.

Table III. Calculated electron contamination in scattered pion beam conversion and Dalitz electrons.

θ_{lab} (deg)	Conversion electrons per I. V.[a]	Dalitz electrons per I. V.
20	29.4	19.4
30	23.3	15.1
40	17.8	11.1
50	13.1	8.1
60	9.5	5.9
70	6.5	4.0
80	4.7	2.7
90	3.7	2.0
100	3.2	1.7
110	3.0	1.5
120	2.9	1.5
130	2.8	1.5
140	2.8	1.6
150	2.8	1.6
160	2.8	1.6
170	2.8	1.7

[a] 1 I. V. represents approx 93×10^6 incident pions. The laboratory DCS is plotted in Fig. 10, using this unit, for comparison.

At several angles, voltage plateaus of all counters were checked. The accidentals mentioned previously were checked with target full and empty and found to be negligible at all angles. Data were taken at several angles with the counter telescope at varying distances from the target, thus giving a solid angle other than the "normal" one. The value of the cross section obtained in this way was in agreement with the value with data taken at the "normal" solid angle. Data taken at full beam level were checked at lower beam levels throughout the duration of the experiment and found to be independent of beam level.

3. Simultaneous Experiment

While this experiment was being carried out on one side of the hydrogen target, an experiment for measuring the polarization of the recoil proton in the π^--p scattering process was being carried out on the side of the target.[4] In order to avoid possible changes in background level, all data cycles were taken during periods when no changes were being made in the polarization experiment.

Approximately halfway through the experiment, the DCS experimental setup and the polarization setup were exchanged.

D. Normalization Measurement

A pion beam of intensity greater than 10^6 pions/sec was necessary to achieve the accuracy desired in the DCS measurement. Such an intense beam cannot be counted by scintillation counters because counting losses are prohibitive with the usual cyclotron duty cycle and present μsec resolving times of coincidence circuitry. Therefore the DCS data were taken while the incident pion beam was being monitored with an ionization chamber.

It was felt, however, that is accurate measurements of the DCS could be made at a few angles while monitoring the incident beam with counters, this would make for a more accurate determination of the overall normalization of the DCS than with the ionization chamber alone.

Such a measurement became feasible with the completion of the auxiliary dee of the Berkeley 184 inch cyclotron, which increases the duty cycle by roughly a factor of 25 and in turn allows much higher counting rates in beam counters with negligible counting losses.

1. Experimental Arrangement

No changes were made in the beam or target during the normalization run. The ionization chamber was replaced by counters A and B as shown in Fig. 4. The dimensions of the counters are given in Table I.

The electronics schematic is shown in Fig. 6, the block shown within the dashed line being essentially the same as in Fig. 5. The signals from counters A and B were delayed with respect to the counter telescope and amplified. They were then fed into a Wenzel-type coincidence[13] with an 8×10^{-9} sec resolving time. The output of the coincidence circuit was amplified and then split, half the signal driving a 40-Mc discriminator-scaler unit, and the other half being put into coincidence with the counter telescope in the Garwin-type coincidence circuit.[10] The output of this circuit was fed into a 10-Mc discriminator unit,[11] which in turn fed uniform pulses to the 10-Mc scaler units.

2. Experimental Procedure

In the normal operation of the cyclotron the main pion beam exhibits a structure in time which reflects the accelerating characteristics of the 184 inch cyclotron. The repetition rate of 64 accelerations per second gives 64 groups of pions per second, each of which is composed of fine-structure pulses having a width of about 5×10^{-9} sec and equally spaced at 52×10^{-9} sec. This spacing corresponds to a final rf accelerating frequency of 19.2 Mc/sec. The duration of the coarse groups is about 300 μsec, and this time is equally filled with beam, thus containing about 3.6×10^{5} rf pulses per second. Since pions in the same rf pulse cannot be resolved electronically, it is impossible to count more than about 4×10^{4} pions/sec, with counting losses < 1% with counters situated in this beam.

However, when the cyclotron is operated with the auxiliary dee, the 64 bunches of pions per sec can be spread out in time over a period of 8 msec each, rather than the 300-μsec period under "normal" operation.

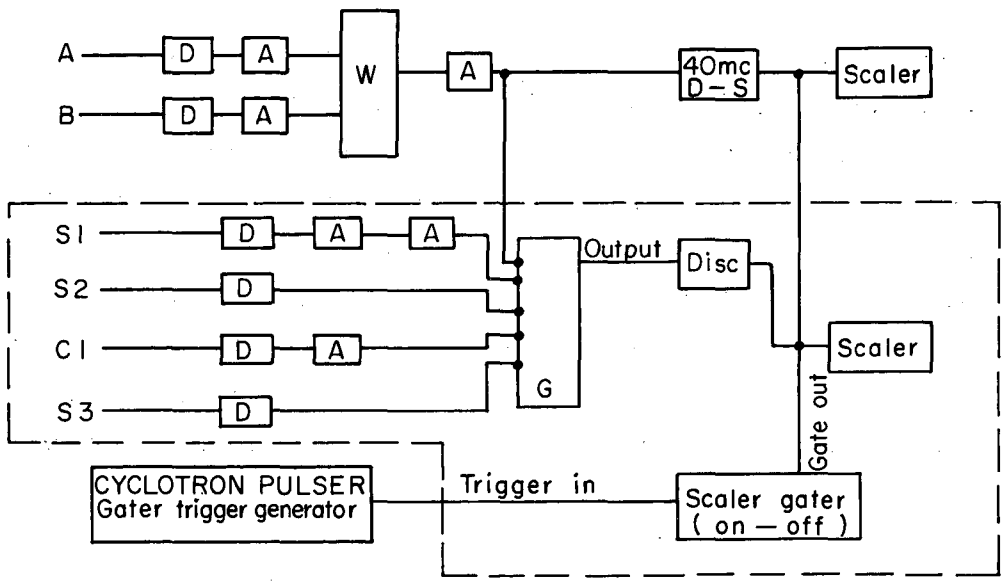

MU-27128

Fig. 6. Block diagram of the electronics used in "normalized" DCS measurement: A = H-P460A amplifier; D = 125Ω delay box; G = Garwin multiple-input coincidence circuit; Disc = 10 Mc/sec discriminator unit; W = Wenzel coincidence circuit; D-S = 40 Mc/sec discriminator-scaler unit.

However, it was found that about 40% of the beam in the 8-msec period was located in a 200-μsec "spike" at the beginning of the period. The remaining 60% of the beam was equally spaced in the remaining time interval. It was necessary to gate the scalers off for the duration of this spike for each of the 64 bunches of pions per sec.

With the new "stretched" beam we have about 8×10^6 rf pulses/sec, which will allow counting rates of about 10^6 pions/sec with small counting losses. We were then able to obtain accurate measurements (2% to 3% counting statistics) of several DCS points in a reasonable length of time, by monitoring the beam with counters.

During the experimental run the counting rate in beam counters was varied from about 1 to 3×10^5 pions/sec. The beam time characteristics and the scaler gating were continuously displayed on a dual-beam oscilloscope. Periodic checks of counting losses were made by delaying counter A with respect to counter B by 52×10^{-9} sec. The counting losses were always $\leq$ 0.1% of the counting rate. Cross-section measurements were made with the counter telescope at three lab scattering angles of 50, 90 and 145 deg.

Each cycle consisted of a target-full and target-empty run, and a run on both a full and empty target with the beam counters delayed by 52×10^{-9} sec with respect to the counter telescope. This coincidence rate measured the accidental rate between the telescope and beam counters. A correction to the data was made for this accidental rate, which was less than 2% of the normal counting rate at all angles.

A list of cross-section data obtained in this normalization run is given in Table IV.

Table IV. Results of normalization measurement.

θ_{lab} (deg)	$\theta_{c.m.}$ (deg)	Normalization $\frac{d\sigma}{d\omega}\Big\vert_{cm}$ (mb/sr)	Lead-squares fit (counts/I. V.)	Counts/I. V. / (mb/sr)
50	66.8	0.948±.029	135.9	143.4±4.2
90	109.8	0.447±.019	66.8	149.6±6.5
145	155.2	0.941±.022	130.8	138.9±3.3
		Average (counts/I. V.)/(mb/sr) =		141.8±2.4

III. DCS RESULTS

A. Corrections to Data

A number of corrections must be made to the raw data before a DCS can be extracted from it. One purpose of this experiment was to keep these corrections as small as possible, consistent with performing the polarization measurements (described in Sec. II. C.3) at the same time. A description of these corrections is given below.

1. Electron Contamination in the Scattered Pion Beam

As mentioned in Sec. II. C. 1, decay of the neutral pion produced by charge-exchange scattering in the hydrogen target gives rise to an electron contamination of the scattered pion beam which is counted in the counter telescope. This contamination results from two different decay modes of the π^0. This main decay mode, which occurs approximately 99% of the time, is

$$\pi^0 \rightarrow \gamma + \gamma. \tag{3.1}$$

These γ's produce $e^+ + e^-$ pairs by interacting with the material between the point of their production and the counter telescope. Either member of this pair may count in the telescope. For convenience, the electrons arising from this mode of decay are here called conversion electrons.

A rarer decay mode of the π^0 is the production of a Dalitz pair,[12]

$$\pi^0 \rightarrow \gamma + e^+ + e^-. \tag{3.2}$$

In this case too, either member of the Dalitz pair may count in the telescope. Again for convenience, the electrons arising from this decay mode are called Dalitz electrons in this paper.

A calculation of these electron contaminations has been made and the data corrected for them. The calculation for both the conversion and Dalitz electron contaminations is described below.

a. Conversion-Electron Contamination. In order to calculate the number of conversion electrons counting in the counter telescope as a function of lab scattering angle, three major pieces of information must be obtained by experiment or calculation. These are:

(a) The γ-ray distribution from the charge-exchange reaction at 310 MeV,

(b) The conversion efficiency for these γ's, of the material between the scattering center and the counter telescope at all angles, and

(c) The number of those $e^{\pm}$ produced that will count in the counter telescope.

The information on the γ distribution can be obtained from a measurement of the charge-exchange cross section. Such a measurement has been carried out near 310 MeV by Caris at 317 MeV incident π^- energy,[5] and by Zinov and Korenchenko at an incident energy of 307 MeV.[6] The two experiments are essentially in agreement. The γ distribution can be obtained from the charge-exchange DCS in a familiar way.[6]

The coefficient fit used for the γ distribution in the c.m. system was that measured by Caris:[5]

$$\frac{d\sigma_\gamma}{d\omega} = \sum_{\ell=0}^{2} b_\ell P_\ell, \tag{3.3}$$

where the P_ℓ's are the Legendre polynomials, and the b's are given by

$$b_0 = 2.80 \pm 0.12,$$

and

$$b_1 = 2.93 \pm 0.16,$$

$$b_2 = 1.78 \pm 0.19.$$

This γ distribution was transformed into the laboratory system; it is shown in Fig. 7.

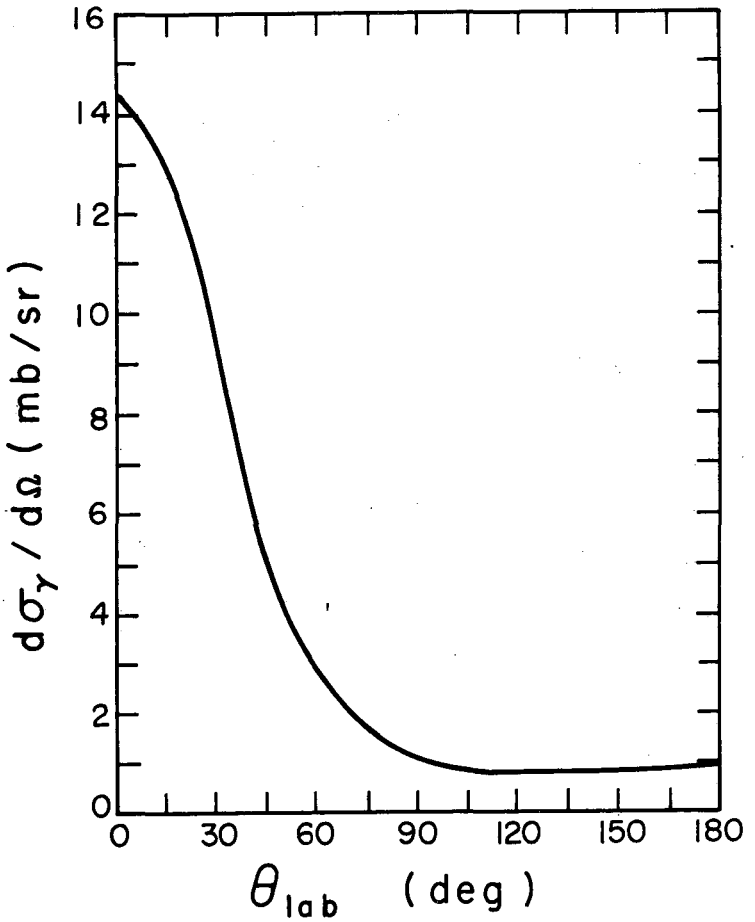

MU-27125

Fig. 7. Laboratory-system γ distribution from charge-exchange scattering at 317 MeV.

The conversion efficiency of the material between the scattering center and the counter telescope was calculated in the following way:

Essentially all the γ's produced from the π^0 in the charge-exchange reaction are of sufficiently high energy that only pair production is important. This effect can be characterized by a parameter known as the mass absorption coefficient, which is a function of the γ-ray energy and the composition of the material. The number of γ's transmitted by a block of material x g/cm^2 thick is given by the equation

$$N_\gamma = N_\gamma^0 \quad \exp[-\alpha x], \tag{3.4}$$

wheren N_γ^0 is the number of γ's with energy k entering the block of material, and α is the mass absorption coefficient for that material and that energy γ-ray. The number of $e^+ + e^-$ pairs formed per incident γ, N_p/N_γ^0, in a thin block of material x (g/cm^2) thick is given by

$$\frac{N_p}{N_\gamma^0} \approx \alpha x . \tag{3.5}$$

The problem is complicated, in this case, by the fact that in the laboratory system the γ's are not monoenergetic at a given angle. Also, the γ's pass through a number of different materials. Therefore, to calculate by Eq. (3.5), the number of pairs produced at a given angle an average value of α must be obtained at each angle and for each material. The average value of α as a function of lab angle was obtained by weighting α by the energy and angular distribution of the γ's in the laboratory system:

$$\bar{\alpha}_i(\theta) = \frac{\int \alpha_i(k) \frac{d^2\sigma}{dk d\Omega} dk}{\int \frac{d^2\sigma}{dk d\Omega} dk}, \tag{3.6}$$

where k is the γ energy and the subscript i is to indicate that this averaging must be done for each material. The double differential cross

section $d^2\sigma/dkd\Omega$ gives the angular and energy distributions of the γ's in the laboratory system.

An IBM program ALPHA BAR calculates $d^2\sigma/dkd\Omega$ from the charge-exchange cross section and kinematics. Values of $\alpha_i(k)$ taken from the literature[15] are input to the program for various materials. ALPHA BAR then calculates $\bar{\alpha}$ as a function of lab angle by performing the integration in Eq. (3.6) numerically for each material. The conversion efficiency can then be calculated as

$$\text{Conv. eff.} \equiv \frac{N_p}{N_\gamma^0} = \sum_i \bar{\alpha}_i \bar{x}_i , \tag{3.7}$$

where the summation is over the materials in the path of the γ's. The conversion efficiency varies between 1.1% and 1.3% over the lab angular region.

The number of electrons that will count at a given lab angle must now be calculated. This can be done with a knowledge of the opening angle between the members of the energy-angular distribution of the γ's that produce the pairs. The opening angle of the pair is a function of the energy of the γ that produced it and the sharing of this energy by the members of the pair. The opening angle of the pair as a function of the incident γ energy and energy-sharing of the pair has been calculated by Borsellino.[16] The energy sharing as a function of incident γ energy and conversion material has been calculated by Heitler.[17] This information, in conjunction with the γ energy-angular distribution calculated by ALPHA BAR, is then used to calculate the number of electrons that will count at each lab angle.

The number of conversion electrons counted per unit of incident pions is shown plotted against lab angle in Fig. 8. The shape of the curve is, as expected, very close to that of the lab γ angular distribution (see Fig. 7).

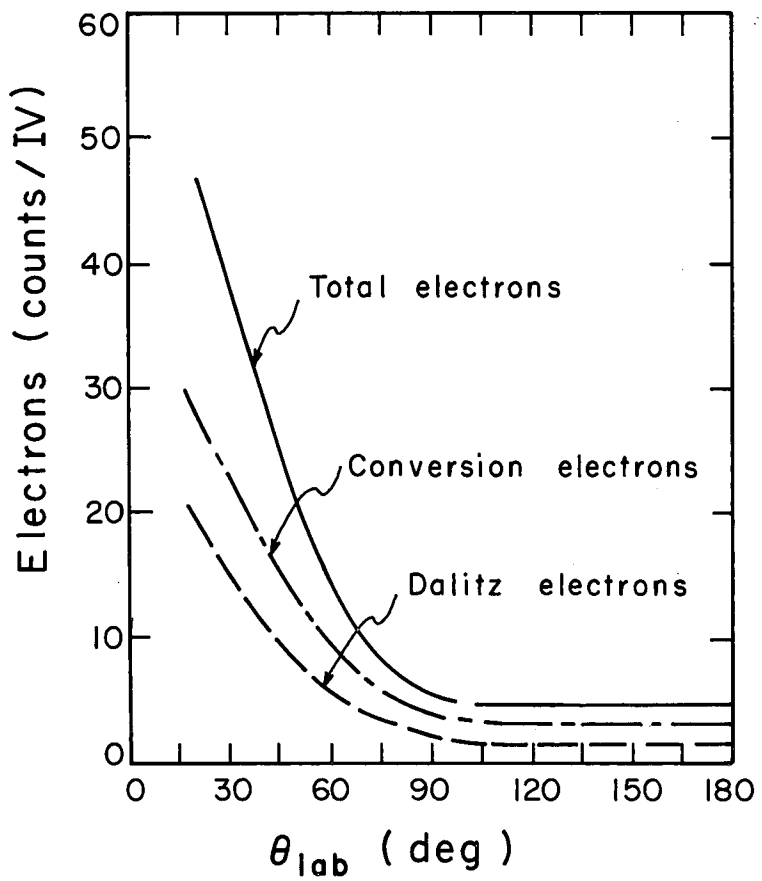

MU-27120

Fig. 8. Electron contamination in the scattered pion beam as a function of laboratory-system scattering angle.

b. Dalitz Electron Contamination. The calculation for the Dalitz electrons was made in roughly the same manner as the conversion-electron calculation. This calculation can also be separated into three parts:

(a) the angular distribution (lab) of the Dalitz pairs must be determined,
(b) knowledge of the branching ratio for this decay mode and the γ-ray cross section allows a calculation of the number of $e^{\pm}$ pairs produced, and
(c) the fraction of the electrons that will count in the telescope must be determined.

The angular distribution of the Dalitz pairs was assumed to be identical to the γ angular distribution. There is evidence that this is a good assumption.[18, 19]

The branching ratio R has been accurately calculated by Josephs.[18] It has also been measured by Derrick et al.[19] and the measurement is in agreement with the theoretical value. Josephs obtained

$$R = \frac{\pi^0 \rightarrow \gamma + e^+ + e^-}{\pi^0 \rightarrow \gamma + \gamma} = 0.01196.$$

The differential cross section (lab) for the pairs can then be written as

$$\left.\frac{d\sigma}{d\Omega}\right|_{\text{pairs}} = \frac{1}{2} R \frac{d\sigma_\gamma}{d\Omega} . \tag{3.8}$$

As in the conversion-electron case, in order to calculate the number of Dalitz electrons that will count in the counter telescope, a knowledge of the opening-angle distribution is needed. Once it is obtained, a calculation of the probability of the pair contributing one or two counts to the angular distribution can be made. The calculation is made in much the same way as that for the conversion electron.

The opening-angle distribution has been calculated by Dalitz[12] and experimentally verified by Derrick et al.[19] After a transformation to the laboratory system, this distribution can be used to make the desired calculation.

The results of the calculation are shown in Fig. 8. The sum of the conversion and Dalitz electron counts in the telescope is also shown. Figure 9 shows a smooth curve of the lab π^- angular distribution, for comparison. The electron contamination is maximum at forward angles. For a 30-deg lab angle the conversion electron correction is 8%, and the Dalitz electron correction is 5%. In the backward direction, the Dalitz electron correction falls to 2% and the conversion electron correction to 4%. These calculated corrections were applied to the data.

2. Counter Telescope Efficiency

The counter telescope S1 S2 C1 was not 100% efficient. At angles forward of 70 deg copper was put before counter C1 to allow the latter to discriminate against inelastic pions produced in the target, as described in Sec. II. B.1. The measured efficiency corrected for contaminants in the incident and scattered beams is given in Table II, along with the amount of copper used at each angle.

A much smaller correction for efficiency had to be made because a few pions scattered toward the defining counter S2 did not register a coincidence in the telescope. This was caused by an interaction in one of the counters that scattered the pion so it did not pass through all three counters of the telescope. The counter telescope was essentially, however, 100% efficient for counting pions that were not scattered out of it. This efficiency varied with angle, primarily because of the variation of pion energy with scattering angle. The efficiency was calculated by using the data of Sternheimer.[20] It varied from 98.5 to 97%. It was checked at forward angles as mentioned in Sec. II. B.2, and at a few backward angles by fastening various additional thicknesses of scintillator to counters S1 and S2, and extrapolating to zero thickness. The counting statistical errors for these effects were significantly large (1/3 to 1/2 the effect) but the measured values were in agreement with the calculation. A correction was made to the data for this effect, as well as for the attenuation in copper at forward angles.

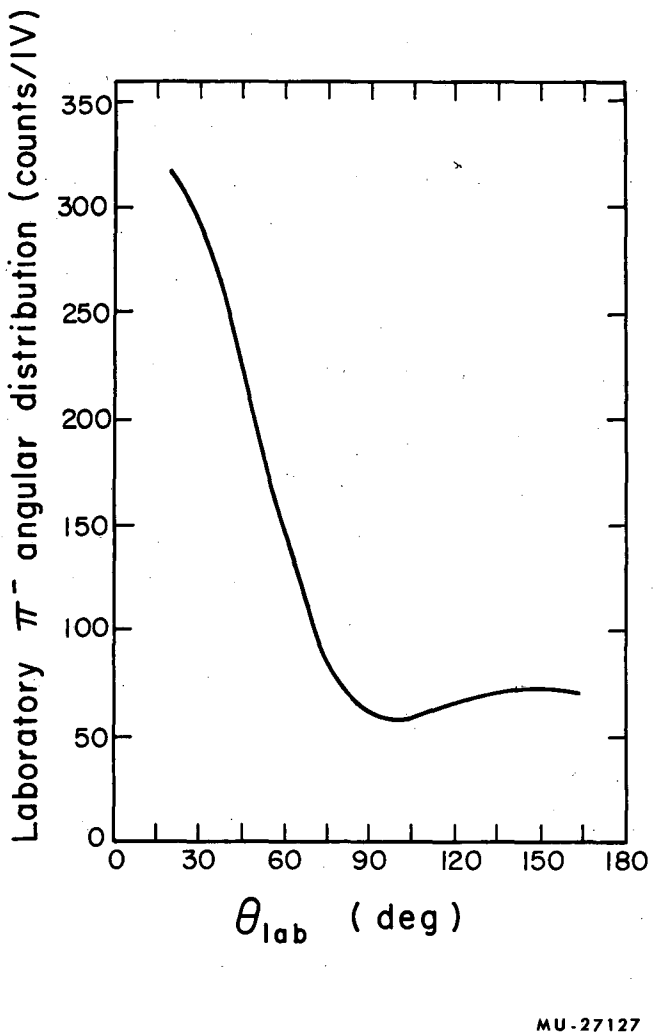

Fig. 9. Smooth curve of laboratory-system π^- angular distribution vs scattering angle.

3. Finite Target and Telescope

A correction must be made for the fact that the target and defining counter are not point objects. The correction for the effective solid angle subtended by the finite counter telescope from a finite target was made by considering division of the target and the defining counter of the telescope first as made of up four and then of twelve parts, and summing their individual contributions. The result for both cases amounted to no more than 0.5% correction at any angle.

A correction had also to be made for averaging the DCS over the finite angular width of the counter telescope. This correction was significant only for scattering angle near 70 deg, where the curvature of the DCS is relatively large. Even here the correction was less than 1%. This correction was also applied to the data.

4. Other Corrections

Several other small corrections to the data were necessary. After the pions scatter once in the hydrogen, they have a finite chance to undergo a second scattering before they leave the hydrogen target. If they undergo direct scattering in the hydrogen during the second scattering, i.e.,

$$\pi^- + p \rightarrow \pi^- + p, \tag{3.9}$$

a slight distortion of the angular distribution results. This gives rise to less than 0.5% correction at all angles. If the pions undergo charge-exchange scattering during the second scattering, i.e.,

$$\pi^- + p \rightarrow \pi^0 + n, \tag{3.10}$$

they become lost and the angular distribution is lowered by a slight amount. The correction for this effect varies from 0.5 to 1.25% over the angular region measured. This calculated correction has been applied to the raw data.

Several other small corrections due to multiple scattering and attenuation of the incident pion beam between the monitors and hydrogen target were calculated and found to be less than a few tenths of 1% and hence were neglected. The distortion of the angular distribution because

of the scattered pions decaying into muons was found to be less than 0.2%, and was also neglected.

B. Normalization Corrections

Corrections to the data taken during the normalization run (Sec. II.D.) must also be made. Since the method of detecting the scattered pion was no different from that used in the cross-section measurement, all corrections that applied to the cross-section measurement (previous section) were exactly the same for this measurement. The only correction that must be made in addition is one taking into account the contaminants in the incident beam, which consisted of electrons and muons. The electron contamination was measured by placing a gas Cerenkov counter at the approximate position of the hydrogen target in line with the beam counters A and B. This gas Cerenkov counter, described elsewhere,[9] was filled with sulfur hexafluoride. It had a threshold of $\beta=0.99$, and since the incident pions and muons had β's less than this value, only electrons were counted by this counter. It was put into coincidence with A and B and the ratio A, B, CG/A, B measured. The electron contamination amounted to 0.3% of the incident beam.

There were two principal sources of muon contamination in the incident beam. One was from the region of the internal beryllium target and the other from the decay of the pions just before counter B. Only those muons produced near the internal beryllium target with a momentum near 430 MeV/c would be transmitted by the magnet system. Muons having the same momentum as pions have a longer range in copper, and hence stand out as a bump on a range curve (Fig. 3). The muons visible at this range makeup 4% of the incident beam. However, a calculation based on a paper by Sternheimer[21] indicated that for the geometry and absorber used, about 10% of the muons are scattered out of the backup counter by multiple Coulomb scattering. Thus, this muon contamination comprised 4.5% of the incident beam.

In the region between the bending magnet M1 and the defining beam counter B, some of the muons from the decay of the pions may register a coincidence in A-B and hence be indistinguishable from a pion A-B coincidence. The muons from the decay of 428 MeV/c pions are confined to a

cone of half-angle 5.3 deg with respect to the incident pion direction, with most of the muons found near the edge of the cone. Thus, only muons from pions that decay within a few feet of counter B have an appreciable probability of counting in B. The momentum of these muons is uniformly distributed between 240 and 430 MeV/c, and so they are impossible to identify on a range curve. The result of this calculation is that 2.7% of the beam is made up of muons of this kind.

A small correction was also made for pions that count in A and B and then decay into muons before entering the liquid hydrogen target. This effect is responsible for an 0.8% contamination of the incident beam.

Thus, a total of 8.3% of the incident flux does not consist of pions and was excluded from the calculated incident pion flux.

C. Differential Cross Section

1. Scattered Pions Counted

The number of scattered pions counted per incident pion was determined for each angle by taking the raw data measured at that angle (see Sec. II. C.2) and subtracting the counts per incident pion with the target empty from the counts per incident pion with the target full, for each full-empty cycle. The value obtained at each angle was the average rate of all cycles at that angle, weighted by the counting statistics in the usual way. The corrections described in Sec. III. A were then applied to to these data and a final lab counting rate as a function of lab angle obtained. This curve is shown in Fig. 10.

2. Target Constant

The lab differential cross section is related to the average scattered pion per incident pion, N_s/N_i, by the equation

$$\frac{d\sigma(\theta)}{d\Omega} = \frac{N_s(\theta)}{N_i \Omega T}, \tag{3.11}$$

where N_i is the number of incident pions, and N_s is the number of pions scattered into a counter that subtends a solid angle Ω as seen from the

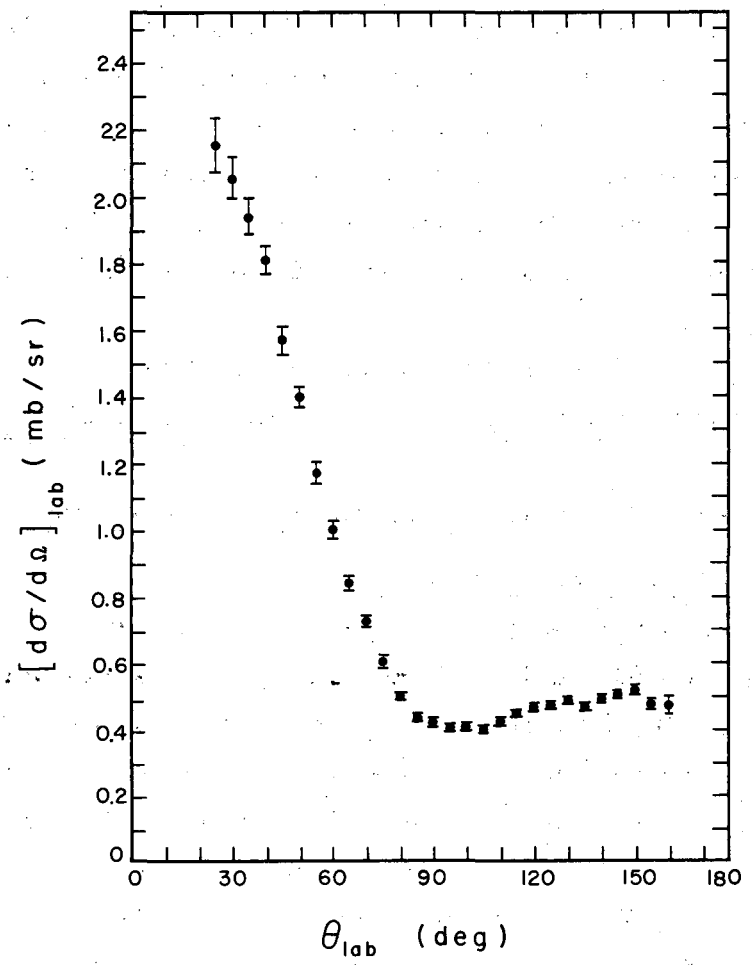

MU-27123

Fig. 10. 310-MeV π^- DCS plotted vs scattering angle in the laboratory system.

target, and lying at an angle θ with respect to the incident pion direction. The target constant, T is the effective thickness of the target in protons/cm^2. For hydrogen, we have

$$T = \frac{N_0 \rho L}{M} , \tag{3.12}$$

where N_0 is Avogadro's number, and M is the atomic weight of hydrogen; ρ is the effective density of hydrogen, and L is the effective length of the target. The effective hydrogen density used was taken as the difference between target-full liquid and target-empty vapor. These densities were obtained from the Cryogenic Data Book.[22] The liquid density was taken as 70.2 g/l, the density of boiling liquid hydrogen. It was assumed that the vapor had a temperature between those of liquid hydrogen and of liquid nitrogen. The vapor density chosen was 0.9 g/l. The value thus obtained for ρ was 69.3 g/l. The effective thickness of the target, L, was obtained by measuring the diameter of the cylindrical flask with a pressure 1 atmos greater inside the flask than outside, the approximate condition under which it operated during the experiment. This was done at room temperature and at liquid nitrogen temperature. A linear extrapolation was made to liquid hydrogen temperature. This thickness was averaged with weights determined by beam profile measurements (Fig. 3) to obtain the effective target length, which was determined to be 14.85 cm. The value of the target constant was calculated to be 6.16×10^{23} protons/cm^2.

3. Normalization

The lab angular distribution data were transformed into the c.m. system with the aid of a kinematics program called KINE. To obtain an accurate normalization of the DCS, the data from the three normalization points measured during the experiment were used (see Sec. II.D) in the following way:

The lab differential cross sections at all three points were calculated, by using Eq. (3.11) after all corrections had been made to the data. These cross-section points were then transformed to the c.m. system.

A least-squares fit of a power series in $\cos\theta_{cm}$ (where $\theta_{c.m.}$ is the c.m. angle) was made to the 28 c.m. angular distribution points. This resulted in a smooth "best fit" curve for all center-of-mass angles. The values of the angular distribution points (in units of counts per I.V. (1 I.V. is equal to 10^{-8} Coulombs of charge collected from the ionization chamber) were taken from this curve at the three angles where the normalization DCS measurement had been made. Comparison of the angular distribution points and the absolute cross section points is made in Table IV. The average value of the ratio (counts/I.V.)/(mb/sr) was used to normalize the angular distribution.

An absolute calculation of the DCS was also made by using the ionization chamber alone. The absolute scale of the DCS measured with the ionization chamber had an uncertainty of about 6%, while the normalization procedure described above resulted in about a 3% uncertainty in the absolute scale factor. The scale factor as determined by the ionization chamber differed from that determined by the normalization procedure by 3.5%.

A list of the DCS vs c.m. scattering angle is given in Table V. A graph of the data is shown in Fig. 11.

Table V. π^--p differential cross section in the center-of-mass system.

θ_{lab} (deg)	$\theta_{c.m.}$ (deg)	DCS (mb/sr)	Percentage error due to counting statistics only
25	34.7	1.184±.043	2.5
30	41.4	1.171±.035	1.4
35	47.9	1.151±.033	1.5
40	54.4	1.125±.029	1.5
45	60.6	1.027±.027	1.7
50	66.8	0.970±.023	1.4
55	72.7	0.853±.023	1.8
60	78.5	0.774±.018	1.6
65	84.1	0.690±.018	2.1
70	89.6	0.635±.015	1.9
75	94.9	0.561±.017	2.6
80	100.0	0.498±.013	2.2
85	105.0	0.461±.014	2.7
90	109.8	0.480±.009	1.5
95	114.5	0.482±.016	2.9
100	119.0	0.514±.012	1.8
105	123.5	0.536±.013	2.0
110	127.8	0.590±.018	2.7
115	132.0	0.663±.019	2.5
120	136.0	0.715±.016	1.9
125	140.0	0.764±.021	2.7
130	144.0	0.822±.020	2.3
135	147.8	0.817±.021	2.4
140	151.6	0.889±.025	2.7
145	155.2	0.941±.015	1.4
150	158.9	0.991±.028	2.5
155	162.4	0.932±.029	2.7
160	166.0	0.944±.042	4.2

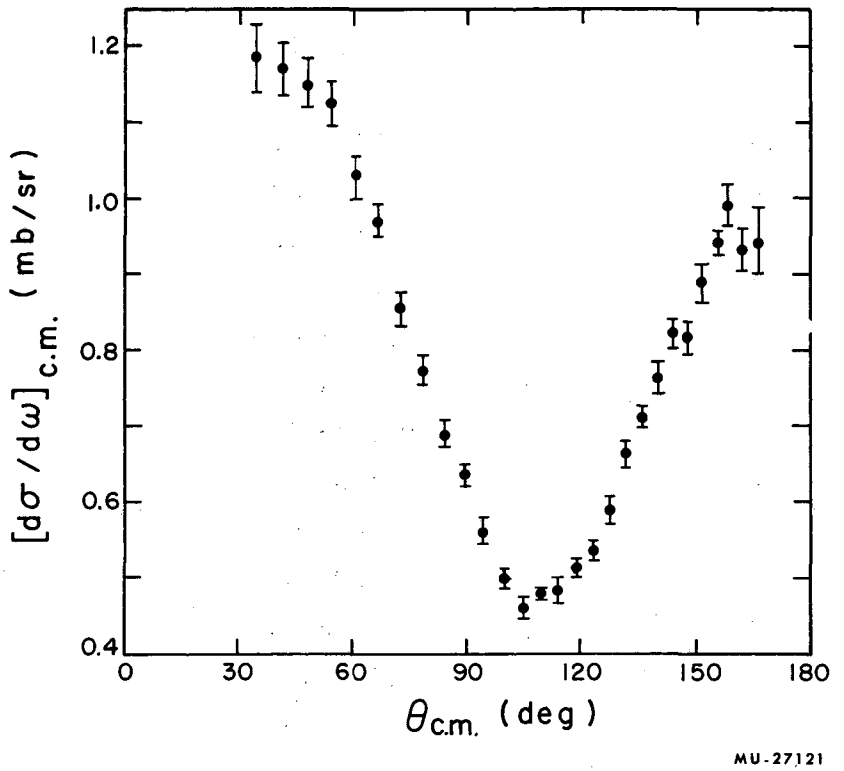

Fig. 11. 310-MeV π^- DCS plotted vs scattering angle in the center-of-mass system.

D. Errors

The uncertainties associated with the DCS measurements fall into three natural catagories:

(a) counting statistics,

(b) absolute DCS scale, and

(c) corrections.

The counting statistics were determined in the usual manner, through the formula

$$\Delta\left(\frac{N_s}{N_i}\right) = \left[\frac{N_s(\theta)}{N_i^2}\Big|_{\text{full}} + \frac{N_s(\theta)}{N_i^2}\Big|_{\text{empty}}\right]^{1/2} . \qquad (3.13)$$

A list of the percentage error in the DCS due to counting statistics is found in the last column of Table V. The error in the absolute cross section scale is due mainly to statistical counting errors on the normalization points (1.5%), uncertainty in the target constant (about 2.0%) because of possible errors in density of hydrogen–especially the gaseous hydrogen temperatures–and in the size of flask. The error in the determination of the solid angle is negligible.

A parameter ϵ was introduced to express the uncertainty in the absolute DCS scale. The data are thus presented as $(d\sigma/d\omega)(1+\epsilon)$, where the most probable value of ϵ is zero. The error on ϵ is estimated to be 3%.

Errors due to various corrections to the data are the most difficult to estimate. The main uncertainty comes from the calculation of the electron contamination in the scattered pion beam. It was estimated that because of uncertainties in the data used and approximations made, an error of between 15% and 20% of the magnitude of the correction should be attached to this calculation. The uncertainties in the corrections for telescope efficiency, finite counter and target size, etc., result in essentially negligible errors for most of the DCS points; however, the corrections

themselves have been included in determining the magnitude of the DCS.

The errors quoted in the DCS points in Table V are a rms combination of the counting statistical error and the electron contamination error.

IV. TOTAL CROSS SECTION

The total cross section σ_T for 310-MeV negatives pions on protons was measured by attenuation. The purpose of this measurement was to gain further information about pion-nucleon scattering at 310 MeV, and to use this information in a phase-shift analysis (see Sec. V). The measurement also gives some information regarding the absolute scale factor ϵ for the differential cross section. This information is not as valuable as it might be because the sum of the reactions, other than the one for which the DCS was measured gives about twice as great a contribution to the total cross section as does the direct scattering process. The processes that contribute to the total cross section are:

$$\pi^- + p \rightarrow \pi^- + p, \tag{4.1}$$

$$\pi^0 + n, \tag{4.2}$$

$$\pi^+ + \pi^- + n, \tag{4.3}$$

$$\pi^0 + \pi^0 + n, \tag{4.4}$$

and

$$\pi^- + \pi^0 + p\,. \tag{4.5}$$

A. Experimental Method

1. Experimental Arrangement

The arrangement of the counters and hydrogen target used to measure the total cross section is shown in Fig. 12. A description of the counters is given in Table I.

The liquid hydrogen target used in this measurement consisted of a 6-in.-diam Mylar flask 12 in. long, surrounded by an aluminum vacuum jacket with Mylar windows at front and back to allow the beam to pass through the target. The beam passed through a total of 0.075 in. of Mylar as well as 12 in. of liquid hydrogen.

The same pion beam was used throughout the experiment. During the total cross-section measurment, the "stretched" beam was used at intensities of about 100 incident pions/sec to ensure a completely negligible accidental rate.

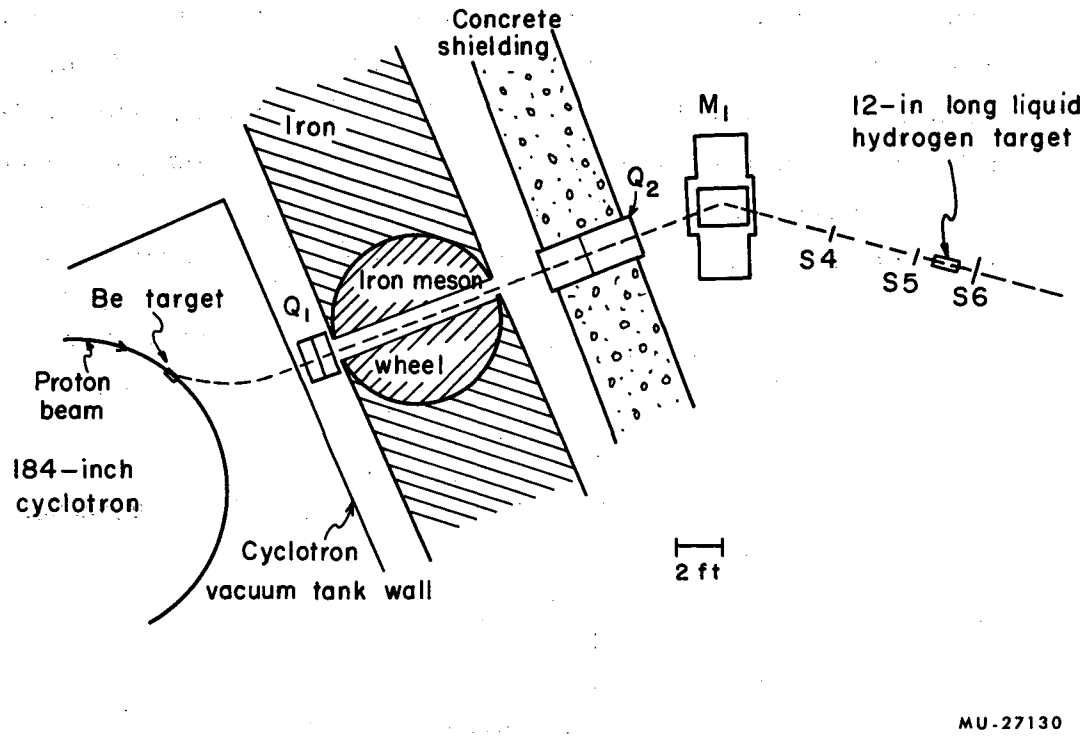

Fig. 12. Diagram of experimental arrangement for the TCS measurement.

2. Experimental Procedure

Four cross-section points were measured as a function of cutoff angle. The c.m. cutoff angle varied from 8.4 to 22.2 deg. The cross section was obtained by taking the ratio S4, S5, S6/S4, S5 with target full and empty at the four cutoff angles. The expression for the total cross section in terms of these ratios, after being corrected for muon and electron contamination in the incident beam, is

$$\sigma_T = \frac{1}{N} \ln \frac{R'}{R}, \tag{4.6}$$

where R' is the S4, S5, S6/S4, S5 ratio (corrected) with target empty, and R is the same ratio with target full. Typical ratios were R = 0.955, and R' = 0.985. The target thickness N is in protons/cm^2.

In addition to the correction for contaminants in the main beam, a very small correction was made in cutoff angle to take into account the finite size of the target. All other corrections were negligible. The data taken at all angles were obtained with one coincidence circuit measuring S4, S5, S6 and the other S4, S5 for half a run; then the circuits were switched and data taken in that fashion again for the remainder of a run. Although the circuits tracked to better than 1 part in 1000, a slight uncertainty was introduced into this measurement at some cutoff angles because of the circuit's inability to track exactly.

B. Results and Errors

The results of the total cross-section measurements are given in Table VI, and plotted vs cutoff angle in Fig. 13. The errors listed are due to counting statistics (≈ 1 to 2%), uncertainties regarding muon contamination, target thickness, and cutoff angle (about 2%), and at certain angles, uncertainty because of failure of the electronics to track exactly.

Also plotted in Fig. 13 are the total cross-section points vs the cutoff angle predicted by the phase-shift analysis when all pion-nucleon data at this energy are used (see Sec. V). These are seen to be in good agreement with the measured values.

Table VI. Total cross section vs c.m. cutoff-angle.

θ^{π}_{cutoff} (deg)	TCS (mb)
8.4	28.8±0.8
11.1	27.5±0.8
13.1	26.7±0.6
22.2	24.6±0.7

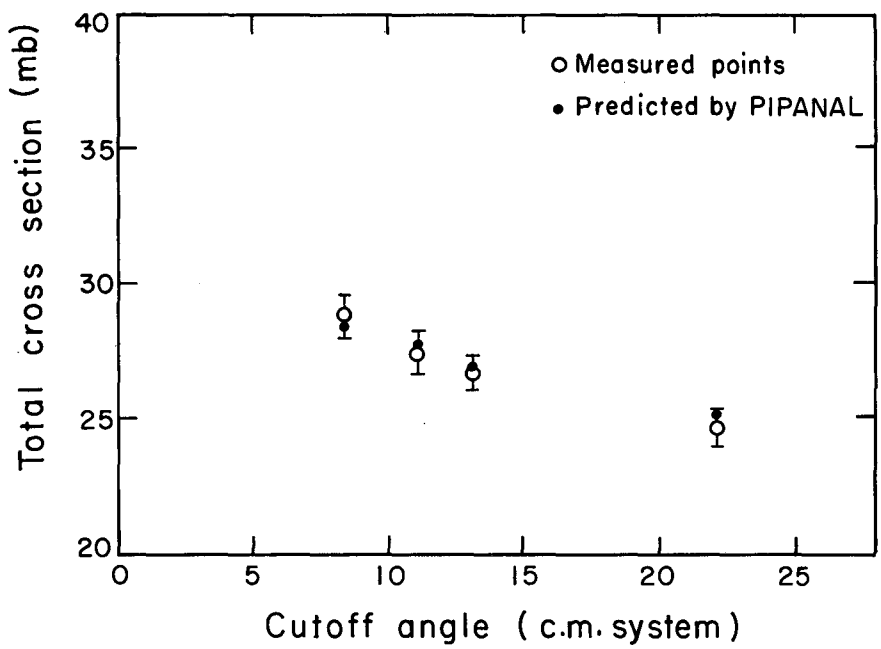

MU-27122

Fig. 13. Graph of the TCS points vs c.m. cutoff angle. The dots represent the cross section predicted by the phase-shift program.

By utilizing the phase-shift analysis, a total nuclear cross section for negative pions or protons can be obtained. Our result was

$$27.7 \pm 0.7 \text{ mb.}$$

This value is in agreement with values obtained by other experimenters at this energy.[23]

V. PHASE-SHIFT ANALYSIS

We completed measurements of the DCS in elastic π^--p scattering at 310 MeV, and obtained data at 28 angles. A measurment of the total cross section as a function of cutoff angle was also obtained. Complementing these results, Olav T. Vik has measured the recoil proton polarization in π^--p scattering at the same energy.[4] In addition, measurements of π^+-p differential and total cross section, and polarization of the recoil proton, had been made previously at this energy by Rogers et al.[1] and Foote et al.,[2] respectively. All these data are noteworthy because of the relatively high accuracy attained. Data from all the above, as well as a measurement of the charge-exchange cross section by J. Caris at 317 MeV,[5] were used in the phase-shift analysis. This section describes the relationship between experimentally measured quantities and the phase shifts, as well as the method and results of the search program that performed the phase-shift analysis.

A. Relationship of Phase Shifts to Experimental Data

1. Scattering Amplitudes

The expressions for the DCS and polarization of the recoil proton in pion-nucleon scattering are well known (see, for example, Ashkin.[24]) They are usually expressed in terms of a non-spin-flip scattering amplitude g and a spin-flip amplitude h. The DCS expression for pions scattering from an unpolarized proton target is

$$\frac{d\sigma(\theta)}{d\Omega} = |g(\theta)|^2 + |h(\theta)|^2 . \tag{5.1}$$

The expression for the polarization of the recoil proton is given by

$$\vec{P}(\theta) = \frac{2\,\mathrm{Re}\, g^*(\theta)\, h(\theta)}{|g(\theta)|^2 + |h(\theta)|^2}\ \hat{n} = P(\theta)\,\hat{n}, \tag{5.2}$$

where the unit vector is defined by

$$\hat{n} = \vec{k}_{inc} \times \vec{k}_{scat} / |\vec{k}_{inc} \times \vec{k}_{scat}| .$$

The scattering amplitudes are usually expressed as partial-wave expansions. Neglecting Coulomb effects, they can be written as:

$$g(\theta) = \lambda \sum_{\ell=0}^{\ell_{max}} \left((\ell+1) \frac{\eta_\ell^{+} \exp[2i\delta_\ell^{+}] - 1}{2i} + \ell \frac{\eta_\ell^{-} \exp[2i\delta_\ell^{-}] - 1}{2i} \right) P_\ell(\cos\theta), \tag{5.3}$$

and

$$h(\theta) = \lambda \sum_{\ell=1}^{\ell_{max}} \left(\frac{\eta_\ell^{+} \exp[2i\delta_\ell^{+}] - \eta_\ell^{-} \exp[2i\delta_\ell^{-}]}{2} \right) P_\ell^{1}(\cos\theta). \tag{5.4}$$

The definitions of the quantities appearing in Eqs. (5.3) and (5.4) are:

ℓ = orbital angular momentum quantum number,

$\delta_\ell^{\pm}$ = phase shifts for orbital-angular momentum state ℓ and total angular momentum quantum $J = \ell \pm 1/2$,

$\eta_\ell^{\pm}$ = inelastic parameters corresponding to each of the phase shifts.

These quantities are ≤ 1, being equal to unity in absence of inelastic scattering. The use of inelastic parameters allows the phase shift $\delta_\ell^{\pm}$ to be completely real even in the presence of inelastic scattering; in this report the term "phase shift" refers to the real part, $\delta_\ell^{\pm}$. Also, we have

λ = wavelength of either particle in the c.m. system ($\lambda = 1/k$),

$P_\ell(\cos\theta)$ = Legendre polynomial,

and

$P_\ell^{1}(\cos\theta)$ = associate Legendre polynomial defined by

$$P_\ell^{1}(\cos\theta) = \sin\theta \frac{d}{d(\cos\theta)} P_\ell(\cos\theta).$$

The correct expression including the Coulomb corrections is found in Appendix A.

2. Isotopic Spin

If the assumption of charge independence is invoked for pion-nucleon scattering, all possible pion-nucleon reactions can be expressed in terms of four scattering amplitudes; the non-spin-flip and the spin-flip for the two possible isotopic spin states. These two possible I-spin states are $I = 3/2$ and $I = 1/2$. The π^+-p system must be all $I = 3/2$, since $I_3 = +1$ for the π^+ and $+1/2$ for the proton, giving an I_3 of $+3/2$ for the system.

The π^--p system, however, has $I_3 = -1/2$ and hence is a mixture of $I = 3/2$ and $I = 1/2$. The I-spin decomposition of the scattering amplitudes for the three charged-pion proton reactions most studied as shown, for example, in Bethe and de Hoffman[25] are:

Reaction	Scattering amplitudes	
	Non-spin-flip	Spin-flip
(1) $\pi^+ + p \rightarrow \pi^+ + p$	$g(I = 3/2)$	$h(I = 3/2)$
(2) $\pi^- + p \rightarrow \pi^- + p$	$\frac{1}{3} g(I = 3/2) + \frac{2}{3} g(I = 1/2)$	$\frac{1}{3} h(I = 3/2) + \frac{2}{3} h(I = 1/2)$
(3) $\pi^- + p \rightarrow \pi^0 + n$	$\frac{\sqrt{2}}{3}\left[g(I=3/2) - g(I=1/2)\right]$	$\frac{\sqrt{2}}{3}\left[h(I=3/2) - h(I=1/2)\right]$

When these substitutions are made for the non-spin-flip and spin-flip amplitudes in the Coulomb-corrected expressions of Eqs. (5.3) and (5.4), Eqs. (A.3) and A.4) of Appendix A result.

3. Notation

From this point on, the term "phase shift" is employed to mean the nuclear part of the total phase shift (see Appendix A). The notation used here is an extension of the notation used by Foote[3] for the π^+- p system.

The symbol itself denotes the orbital angular momentum state; the first subscript is twice the isotopic spin and the second is twice the total angular momentum, as shown in Table VII.

Table VII. Summary of phase-shift symbols.

		Phase-shift symbol	
ℓ	J	I = 3/2	I = 1/2
0	1/2	$S_{3,1}$	$S_{1,1}$
1	1/2	$P_{3,1}$	$P_{1,1}$
1	3/2	$P_{3,3}$	$P_{1,3}$
2	3/2	$D_{3,3}$	$D_{1,3}$
2	5/2	$D_{3,5}$	$D_{1,5}$
3	5/2	$F_{3,5}$	$F_{1,5}$
3	7/2	$F_{3,7}$	$F_{1,7}$

B. Search Program

1. General Method

Because of their complex relationship to the experimental data, a trial and error method must be used to search for the correct phase shifts. Such a method is ideally suited to the use of modern high-speed computers. An IBM 7090 program has been written to perform this searching function. The general method of this program is outlined below.

A set of phase shifts is input to the computer. The computer is instructed to calculate the desired experimental quantities (the equations in Appendix A were used with this set). The calculated quantities are then compared with the measured quantities. This comparison is made by computing the quantity M:

$$M = \sum_i \left[\frac{X_i^{(c)} - X_i^{(e)}}{E_i} \right]^2 . \tag{5.5}$$

Here $X_i^{(e)}$ is the experimental quantity X_i, E_i is the experimental error (standard deviation) in $X_i^{(c)}$ is the quantity X_i as calculated by the computer for a given set of phase shifts. The summation is made over all experimental measurements.

The program searches for those values of the phase shifts which give a relative minimum to this quantity M. This "least-square" minimization is carried out by the grid search method,[26] in which the phase shifts are varied by fixed amounts (size of grid) in cycles. After a relative minimum has been found for each grid size, the search continues with a smaller grid size. Successively smaller changes are made in the phase shifts until the smallest increment by which the shifts are varied is reached. The values of the phase shifts thus obtained correspond to a minimum in M, in the sense that if a change of the smallest grid increment is made in any of the shifts a larger value of M is obtained than the one calculated at the minimum.

The value of M obtained in this manner is only a relative minimum. Also, different initial sets of phase shifts may lead to different minima, some of which may have lower M values.

It is sometimes convenient to visualize the hypersurface that would correspond to a depression in the hypersurface, which may be referred to as a "hole" or "valley" on the surface. This visual representation is often used in the discussion to follow.

The uncertainty in the phase shifts was established by using the error-matrix method, in essentially the manner described by Foote.[3] Additional information concerning this method can be found in the phase-shift analysis discussion by Anderson et al.[27]

The program calculates the quantity G_{ij},

$$G_{ij} = \frac{1}{2} \frac{\partial^2 M}{\partial \delta_i \partial \delta_j} , \tag{5.6}$$

evaluated at the minimum.

The i and j summations extend over all phase shifts. The error matrix G^{-1} is an array of numbers obtained by inverting the matrix G, which consists of a symmetrical array of the quantities G_{ij}. The errors on the phase shifts are related to the elements of the trace of the error matrix as

$$(\Delta\delta_i)_{rms} = \sqrt{(G^{-1})_{ii}} , \tag{5.7}$$

in the obvious notation. It is useful to express the error in any function F of the phase shifts. The rms error in F, ΔF_{rms} is calculated from the error matrix G^{-1} in the formula[28]

$$(\Delta F)_{rms} = \left[\sum_{\ell=1}^{N} \sum_{j=1}^{N} \frac{\partial F}{\partial \delta_i} \frac{\partial F}{\partial \delta_j} (G^{-1}) \right]^{1/2} . \tag{5.8}$$

2. PIPANAL ICF4

PIPANAL ICF4 is the final IBM 7090 program performing the phase-shift search and error analysis. It is the culmination of a long series of programs based on Foote's original π^+-p analysis program.[3]

The general method used by this program has been discussed in Sec. V.B.1; and use in its particular phase-shift investigations is thoroughly discussed in Sec. V.C. In this section we enumerate the quantities that can be varied, and those experimental data that can be fitted with the present program. The notation for these variables and experimental quantities is the same in all three sections.

The quantities in the program that can be varied are:

(a) The isotopic spin 3/2 and isotopic spin 1/2 phase shifts (α and δ respectively).

(b) The isotopic spin 1/2 inelastic parameters (η's); the I-spin 3/2 are not varied from 1.0 because of the small amount of inelastic scattering that takes place in the π^+-p scattering at 310 MeV.

(c) The absolute scale factors for the various DCS's; i.e., ϵ_1 for π^--p elastic DCS, ϵ_2 for π^--p charge-exchange DCS, and ϵ_3 for π^+p elastic DCS. These scale factors take into account possible uncertainties in the knowledge of the absolute normalizations of the various DCS. They serve the same function as the ϵ (which we now call ϵ_1) described in Sec. III.D.

All the above parameters are varied to obtain best fits to the experimental data put into the program. A list of the data that may be put into PIPANAL ICF4 is as follows:

(a) Differential cross section

Up to 30 DCS points for each of the reactions

$$\pi^+\text{-p} \rightarrow \pi^+\text{-p},$$
$$\pi^-\text{-p} \rightarrow \pi^-\text{-p},$$
$$\pi^-\text{-p} \rightarrow \pi^0\text{-n},$$

may be put into the program. If the π^--p $\rightarrow$ π^0-n DCS is obtained by measuring the γ distribution, this DCS is usually expressed in terms of coefficients of Legendre polynomials. It is also possible to insert the data into the program in this form.

(b) Polarization

Up to 10 polarization points may be put into the program for the polarization of the nucleon in the three reactions listed in (a).

(c) Total cross sections

The measured total cross section for one cutoff angle for π^+-p and π^--p scattering can be inserted into the program. The total inelastic cross section may also be used as data.

In addition to printing out the value of M and the phase shifts for the minimum value of M, the calculated values of any of the experimental quantities may be printed for any number of angles.

C. Phase-Shift Investigations

Before the phase-shift analysis was begun, a least-squares fitting program was used to fit the π^--p DCS data. The results of this fitting indicated that the s and p waves alone (i.e., partial waves up to and including $\ell = 1$) could not possibly fit the data adequately. While spd waves gave an adequate fit to the data, the best fit was obtained for spdf waves (i.e., up to $\ell = 3$). For this reason, a phase-shift analysis was carried out for both spd and spdf waves.

The data used for these investigations were:

(a) The data contained in this report; 28 π^--p elastic DCS points, and a total cross-section point for an 8.4 deg cutoff angle.

(b) Four recoil-proton polarization points for π^--p scattering, measured by O. Vik.[4]

(c) Twenty-three DCS points for π^+-p elastic scattering at 310 MeV, and a total cross-section point, all measured by Rogers et al.[1]

(d) Four recoil proton polarization points in π^+-p scattering, measured by Foote et al.[2]

(e) Coefficients for charge-exchange DCS measured by Caris at 317 MeV.[5]

A list of these data is given in Tables VIII, IX, and X. Graphs of the π^- DCS data are given in Fig. 11.

Table VIII.

(a) π^--p differential cross section in the center-of-mass system for 310 MeV.[a]

θ_{lab} (deg)	θ_{cm} (deg)	DCS (mb/sr)
25	34.7	1.184±.043
30	41.4	1.171±.035
35	47.9	1.151±.033
40	54.4	1.125±.029
45	60.6	1.027±.027
50	66.8	0.970±.023
55	72.7	0.853±.023
60	78.5	0.774±.018
65	84.1	0.690±.018
70	89.6	0.635±.015
75	94.9	0.561±.017
80	100.0	0.498±.013
85	105.0	0.461±.014
90	109.8	0.480±.009
95	114.5	0.482±.016
100	119.0	0.514±.012
105	123.5	0.536±.013
110	127.8	0.590±.018
115	132.0	0.663±.019
120	136.0	0.715±.016
125	140.0	0.764±.021
130	144.0	0.822±.020
135	147.8	0.817±.021
140	151.6	0.889±.025
145	155.2	0.941±.015
150	158.9	0.991±.028
155	162.4	0.932±.029
160	166.0	0.944±.042

Table VIII. (continued)

(b) Polarization of the recoil proton in $\pi^- p$ scattering for 310 MeV.

θ_{cm} (deg)	$P(\theta)$
114.2	0.784±.132
124.5	0.648±.076
133.8	0.589±.072
145.2	0.304±.055

[a] The normalization uncertainty was taken to be $\Delta\epsilon = 0.03$.

Table IX.

(a) Differential and total cross sections[a] for $\pi^+ + p \rightarrow \pi^+ + p$, measured by Rogers et al.[b]

θ_{cm} (deg)	$\frac{d\sigma(\theta)}{d\Omega_{cm}}$ (mb/ster)	rms uncertainty (mb/sr)
14.0	18.71	0.60
19.6	16.05	0.46
25.2	13.82	0.31
30.6	12.99	0.25
34.6	12.28	0.27
36.2	11.65	0.27
44.0	9.82	0.15
51.8	8.59	0.26
56.8	7.54	0.28
60.0	6.58	0.22
69.6	4.73	0.10
75.3	3.62	0.09
81.6	2.77	0.08
97.8	1.66	0.07
105.0	1.51	0.06
108.1	1.62	0.07
120.9	2.08	0.08
135.2	2.93	0.14
140.6	3.36	0.12
144.7	3.76	0.15
152.2	4.10	0.21
156.4	4.51	0.17
165.0	4.88	0.12

Table IX (Continued)

(b) Recoil-proton polarization for $\pi^+ + p \rightarrow \pi^+_c + p$ at 310 MeV, measured by Foote et al.[c]

θ_{cm} (deg)	$P(\theta)$	rms uncertainty (mb/sr)
114.2	0.044	0.062
124.5	-0.164	0.070
133.8	-0.155	0.044
145.2	-0.162	0.037

[a] The total cross section used in the analysis was 56.4±1.4 mb, evaluated between cutoff angles 14.7 and 158.0 deg. The normalization uncertainty was taken to be $\Delta\epsilon = 0.06$.

[b] See reference 1.

[c] See reference 2.

Table X. Coefficients for Legendre polynomial fit to $\pi^-_b + p \rightarrow \pi^0 + n$ DCS, measured by Caris[a] at 317 MeV.

$$\frac{d\sigma(\theta)}{d\Omega_{cm}} = \sum_{\ell=1}^{\ell_{max}} A_\ell \, P_\ell(\cos\theta)$$

	Coefficient (mb/sr)	rms uncertainty (mb/sr)
A_1	1.39	0.060
A_2	1.87	0.11
A_3	1.50	0.17
A_4	0.01	0.15
A_5	-0.35	0.42

[a] See reference 5.

[b] The normalization uncertainty was taken to be $\Delta\epsilon = 0.10$.

1. spd Investigations

Most of the searching for phase-shift solutions to the experimental data was done in the following way. Random phase shifts that could vary from -180 to +180 deg were obtained for the I-spin 1/2 phase shifts. These were used as starting points for the I = 1/2 shifts in the search program. Since a phase-shift analysis had already been performed on the π^+-p data,[3] and since a complete random search would have been much too time-consuming, solutions to the π^+-p phase-shift search were used as starting points for the I-spin 3/2 phase shifts. In general, the initial searches were performed by programs simpler than PIPANAL 1CF4 in order to save time. The "good" solutions obtained from these programs were then used as starting points for PIPANAL 1CF4. In the π^+-p phase-shift analysis, Foote found only one solution,[3] which was of the Fermi type that fitted all the π^+-p data adequately ($S_{3,1}$ = 18.5 deg, $P_{3,1}$ = -4.7 deg, $P_{3,3}$ = 134.8 deg, $D_{3,3}$ = 1.9 deg, and $D_{3,5}$ = -4.0 deg). This solution was the starting point for most of the searching. However, some searching was also done with other much less likely π^+-p solutions, which had also been found by Foote. All together, 130 different phase-shift sets were used as starting points in the investigation. This resulted in four acceptable solutions to all the π^+-p data, and the DCS and TCS data, for π^--p elastic reaction. If the recoil-proton polarization data for π^--p scattering as well as the charge-exchange data were used, only one solution giving a reasonable fit to all the data remained. The four solutions for the incomplete data, and the final solution for all the data, are given in Table XI. The next best fit to all the data is also given even though it is statistically an unacceptable solution. The error matrix for the single spd solution that agrees with all the data is given in Appendix B. A study of the effects of various data on the phase-shift errors is shown in Table XII. It will be noted that the addition of polarization and charge-exchange data makes little difference in determining the errors on the phase shifts, but can aid greatly in distiguishing between different sets of phase shifts that fit the other data about equally well. The errors on the spd phase-shift solution vary from 0.4 to 1.1 deg.

Table XI.

(a) spd solutions to π^--p DCS and total-cross-section data (also π^+-p DCS, polarization, and total-cross-section data).

	$M_{expected} = 47$[a]	$S_{3,1}$	$P_{3,1}$	$P_{3,3}$	$D_{3,3}$	$D_{3,5}$	$S_{1,1}$	$P_{1,1}$	$P_{1,3}$	$D_{1,3}$	$D_{1,5}$
(1)	52.4	-18.8	-5.0	134.9	1.7	-3.7	-5.8	-4.0	4.4	-5.3	15.1
(2)	61.3	-18.2	-4.5	135.1	1.9	-4.0	-7.2	25.8	7.3	3.0	-0.5
(3)	57.8	-18.5	-4.7	134.7	1.9	-4.0	4.2	10.5	-2.0	3.6	-0.0
(4)	52.1	-18.9	-5.0	134.3	1.8	-3.9	-4.0	-0.6	5.3	17.3	1.0

(b) spd Solutions to π^-p DCS, polarization, total-cross-section, and charge-exchange coefficients (also π^+-p DCS, polarization, and total-cross-section data).

	$M_{expected} = 56$[a]	$S_{3,1}$	$P_{3,1}$	$P_{3,3}$	$D_{3,3}$	$D_{3,5}$	$S_{1,1}$	$P_{1,1}$	$P_{1,3}$	$D_{1,3}$	$D_{1,5}$
(1)	71.2	-18.8	-4.9	135.5	1.7	-3.6	-6.2	-4.0	3.9	-5.5	15.2
(2)	122.8	-18.5	-4.4	135.5	1.9	-3.9	-3.2	27.7	6.9	2.9	-0.2

[a] $M_{expected}$ means number of degrees of freedom, i.e., the number of experimental points fitted less the minus number of phase shifts varied.

Table XII. Effect of various data on phase-shift errors (spd solution).[a]

Additional π^--p data	Errors (in deg) on I = 1/2 phase shifts				
	$S_{1,1}$	$P_{1,1}$	$P_{1,3}$	$D_{1,3}$	$D_{1,5}$
28 DCS	0.9	0.5	1.3	0.3	0.9
28 DCS, 1 TSC	0.8	0.4	1.0	0.3	0.6
28 DCS, 1 TSC, 4Pol	0.7	0.4	0.9	0.3	0.6
7 DCS[b], 1 TCS, 4Pol	0.8	0.5	1.2	0.4	0.8
7 DCS[b], 1 TCS, 4Pol 5 charge-exchange DCS coefficients	0.8	0.5	1.1	0.3	0.7
28 DCS, 1 TCS, 4 Pol, 5 charge-exchange DCS coefficients	0.6	0.4	0.9	0.3	0.6

[a] All cases include the following π^+p data: 23 DCS points 4 polarization points, and 1 total cross section. In addition, the following π^--p data listed in the lefthand column.

[b] The 7 DCS points are distributed evenly throughout the angular region.

2. spdf Investigations

The spdf analysis closely followed the general procedure of the spd analysis. Again, random phase shifts were used for the input I-spin 1/2 shifts, except for the f waves, which were set equal to zero. The initial I-spin 3/2 shifts were again chosen to be the solutions of Foote's spdf π^+-p analysis. There were two of these solutions, called here Fermi I and Fermi II. The 480 different initial sets of phase shifts, approximately balanced between the two I-spin 3/2 solutions, were fed into the computer with varying amounts of data. When all the π^+-p data and only the π^--p DCS and TCS were used, thirteen acceptable solutions were found; but with the addition of the π^--p polarization data, the number of acceptable solutions was reduced to six. The addition of the charge-exchange data further reduced the number of solutions to three. Finally, two of these three solutions appear to be somewhat more likely than the third.

The three phase-shift solutions are given in Table XIII. The error matrices for these three solutions are found in Appendix B.

Solution I is the spdf counterpart of the only acceptable solution of the spd analysis. It was the most frequently occurring solution, having appeared 37 times during the random search.

Solution II exhibits the Fermi II behavior ($D_{3,3}-D_{3,5} < 0$) of Foote's second solution, but some of the shifts are rather different from those obtained in the π^+-p analysis. Nevertheless, the solution gives a good fit to most of the experimental data. It should be noted that this solution was found only by starting the initial search with Fermi I I-spin 3/2 phase shift sets. No solutions fitting all the data were found by starting the search from Foote's Fermi II solution. We can thus conclude that Foote's Fermi II solution is not an adequate fit to all the data.

Solution III gives a rather poor fit to the data. Statistical arguments[29] indicate that an acceptable solution has less than a 2.5% chance of having an M value as high as that of solution III. Although it is rather unlikely, we have presented it for completeness. All other solutions obtained had a probability of less than 0.5% of being acceptable.

Table XIII

(a) spdf solutions to π^+-p and π^--p DCS, polarization, and total cross section

$M_{expected} = 47$

	M	Started from	$S_{3,1}$	$P_{3,1}$	$P_{3,3}$	$D_{3,3}$	$D_{3,5}$	$F_{3,5}$	$F_{3,7}$	$S_{1,1}$	$P_{1,1}$	$P_{1,3}$	$D_{1,3}$	$D_{1,5}$	$F_{1,5}$	$F_{1,7}$
(I)	37.9	Fermi I	-15.3	0.0	134.8	4.8	-6.4	0.8	-1.6	-5.4	-5.3	2.0	-5.5	15.9	-0.2	2.4
(II)	48.3	Fermi I	-20.7	-10.1	136.1	-2.0	-0.3	-1.1	2.3	11.7	23.4	-2.0	6.7	2.5	2.2	-0.4
(III)	41.3	Fermi I	-15.1	0.1	135.0	4.9	-6.4	0.8	-1.7	-0.2	27.2	7.3	-0.3	-1.6	-2.5	-0.2
(IV)	49.1	Fermi I	-17.4	-2.8	134.2	3.2	-5.1	0.6	-0.8	10.3	20.2	-1.2	5.3	5.7	1.8	0.8
(V)	46.6	Fermi II	-35.5	-16.0	151.3	-11.4	13.0	-1.1	-1.9	-13.0	3.7	19.7	-0.6	-2.0	2.5	1.0

(b) spdf solutions to π^+-p and π^--p DCS, polarization, total cross section, and $\pi^- p \rightarrow \pi^0 n$ DCS

$M_{expected} = 52$

	M	$S_{3,1}$	$P_{3,1}$	$P_{3,3}$	$D_{3,3}$	$D_{3,5}$	$F_{3,5}$	$F_{3,7}$	$S_{1,1}$	$P_{1,1}$	$P_{1,3}$	$D_{1,3}$	$D_{1,5}$	$F_{1,5}$	$F_{1.7}$
(I)	43.7	-14.4	1.1	135.1	5.4	-6.9	0.8	-2.0	-6.0	-5.8	1.5	-5.7	15.8	-0.2	2.5
(II)	64.2	-21.2	-12.1	137.2	-3.3	1.5	-1.8	3.3	10.9	23.1	-3.5	6.5	0.6	2.1	-1.2
(III)	71.7	-15.6	-0.7	135.3	4.2	-6.0	0.7	-1.3	5.0	27.9	9.2	-0.5	-0.7	-3.2	-0.5

3. Inelastic Scattering

All the phase-shift investigations thus far mentioned in this section were carried out assuming the inelastic cross sections for π^+-p and π^--p scattering to be identically zero. This, of course, is not the case. However, for π^+-p scattering, the inelastic cross section is about 0.5 mb[30, 31] compared with the elastic total cross section of about 60 mb,[1] and therefore the assumption that there was no inelastic scattering is quite good. For π^--p scattering the inelastic total cross section is about 1.0 mb,[32, 33] and the elastic total cross section is about 28 mb. Thus, the inelastic cross section is 3 or 4% of the elastic and obviously cannot be neglected. The effect of inelastic scattering on the I-spin 1/2 phase-shift solution has been studied in the following way. The solutions of the spd and spdf analyses were used as starting points for a search with PIPANAL 1CF4. The I-spin 1/2 inelastic parameters were started at 1.0, 0.95, and 0.90 for each solution. An appropriate value of the I-spin 1/2 part of the inelastic π^--p total cross section was used in the program. The result of this analysis was that only a small effect was noted in the phase shifts. The values of the inelastic parameters determined by the program were all ≥ 0.975, with more than half of them being equal to 1.0. These values were essentially independent of their starting point in the program. The I-spin 1/2 phase shifts themselves were not changed by more than the quoted errors on these shifts. The conclusion of this analysis is that, at this energy, inelastic scattering does not play an important part in the determination of the phase shifts.

VI. DISCUSSION OF RESULTS

The basic goal of this experiment, to obtain accurate DCS data for $\pi^- p$ scattering, has been attained. We measured 28 DCS points with counting statistics of about 3%. However, a phase-shift analysis utilizing this and other available data at 310 MeV has not been as satisfactory. Although a single acceptable solution was obtained for spd analysis, all 66 pieces of information available had to be utilized in order to reject all other possible solutions except this one. The extension of the analysis to include f waves was even less satisfactory. The inclusion of even small f waves introduced one and possible two new solutions, which differed markedly in some phase shifts from the spd solution. This may cast doubt on one of the basic assumptions of the analysis, i.e., that higher angular momentum states contribute only very slightly to the interaction at a given energy, and hence may be neglected. In the spdf analysis we have seen that although the f waves are rather small, they have had a considerable effect, introducing solutions rather different from the spd solution.

It appears that in order to choose the correct solution in the spdf analysis, one needs more data. The major limitation of the present pion-nucleon data at 310 MeV is the limited angular region ($114 \text{ deg} \leq \theta_{cm} \leq 146 \text{ deg}$) in which π^--p polarization data exist. Unfortunately, the techniques needed to obtain data at smaller c.m. angles are somewhat different and more complicated than those that used to obtain the existing data. Although such measurements are possible, no data exist at present.

There is theoretical as well as experimental help that might be utilized. It is hoped that a theoretical approach along the lines used in nucleon-nucleon scattering[34] will be developed, and that accurate predictions of the higher angular momentum phase shifts can be made. Chew et al. have used relativistic dispersion relations to make predictions of the $I = 3/2$ and $1/2$ pion-nucleon d-wave phase shifts up to about 300 MeV.[35] These calculations do not contain possible pion-pion interaction effects and so may not describe these phase shifts accurately.

Although some of the d-phase shifts in our solutions do agree with these predictions in sign, the agreement in magnitude is not good, and in fact some of our solutions do not even agree in sign. It is felt that such disagreement should not be taken too seriously until possible π-π effects can be included in the calculation.

Theoretical predictions of the real part of the forward scattering, Re[g(0 deg)], using dispersion relations, have been made by Spearman for π^+-p and π^--p scattering.[36] The values quoted here were for the choice $f^2 = 0.08$, where f^2 is the renormalized, unrationalized, pion-nucleon coupling constant.

For π^+-p, Spearman finds

$$\mathrm{Re}[g(0\ \mathrm{deg})] = -0.69,$$

and for π^--p,

$$\mathrm{Re}[g(0\ \mathrm{deg})] = -0.06,$$

in units of $\hbar/\mu c$, where μ denotes the pion rest mass.

The values of the real part of the forward scattering, as calculated from the spd and spdf solutions, are statistically in agreement with the theoretical prediction listed above.

It appears that, at present, no theoretical or experimental data exist that can resolve the ambiguities in the spdf analysis. However, some progress has been made in the knowledge of the phase shifts at 310 MeV. Previously, there was no accurate information about the I = 1/2 phase shifts at the energy, but now a choice of three individually accurate sets of phase shifts is available. Also, one I = 3/2 solution found by Foote (Fermi II in his notation)[3] was discarded as unable to fit all the data adequately. The basic difficulty brought forth by the analysis is the need for very large amounts of experimental data if accurate information about the phase shifts is desired when d, f, and higher partial waves become important. At 310 MeV the inelastic scattering did not add a serious complication. However, because of the sharp increase in inelastic cross section with energy near 300 MeV,[32] phase-shift analysis at slightly higher energies will become even more

complicated, since appreciable inelastic scattering essentially doubles the number of parameters that must be determined in the analysis. It appears that because of these requirements for very large amounts of data, the method of phase-shift analysis became less useful at these energies than it had been at lower energies. Evenutally, more interest may center on the experimental data themselves and less on the results of the present method of analysis of those data. In this way, it is hoped that the measurements described in this report will make a significant contribution toward the quantitative understanding of the pion-nucleon interaction.

ACKNOWLEDGMENTS

It is a pleasure to acknowledge the continued support of Professor Emilio Segre and of the entire research group under his leadership. The constant optimism and support of Professor Thomas Ypsilantis during this experiment as well as throughout the author's graduate career is greatly appreciated.

To Dr. Olav T. Vik, with whom the author has worked from the beginning of this experiment to the present, must go the greatest appreciation, not only for his able aid during the DCS measurements and his careful measurements of the recoil proton polarization, but for his never-ending willingness to discuss and clarify problems concerning the experiment and phase-shift analysis. His almost unique ability and willingness to work in the early morning hours alone has won the author's eternal gratitude.

The suggestions of Dr. Norman Booth, and numerous discussions with him and with Dr. Ernest Rogers, are gratefully acknowledged. Thanks are due to Mr. David Jenkins for able assistance with tedious calculations and much of the programming chores. Mrs. Patricia M. Brown is to be thanked for her cheerfulness, as well as her accuracy while typing manuscript.

The excellent cooperation and assistance of the 184-inch cyclotron crew under the leadership of Mr. James Vale, as well as the help of accelerator technicians, is gratefully acknowledged.

This work was done under the auspices of the U. S. Atomic Energy Commission.

APPENDICES

A. Inclusion of Coulomb Scattering in Pion-Nucleon Scattering Amplitudes

The scattering amplitudes given by Eqs. (5.1 and (5.2) have been extended to take into consideration the nonrelativistic Coulomb effects, as well as the first-order relativistic Coulomb corrections. This extension was carried out by Foote[3] and was based on the work of Stapp,[37] Solmitz,[38] and Critchfield and Dodder.[39]

In this section we use Foote's Eq. (7) and (8), Sec. B,[3] to write down Coulomb-corrected scattering amplitudes for the reactions listed in our Sec. V.A.2. It will now be convenient to distinguish between phase shifts for states of isotopic spin 1/2 and 3/2. In the following equations (A-1 through A-6) we use the following notation:

$\delta_\ell^{\pm}$ = phase shift for orbital-angular momentum quantum number ℓ, total - angular-momentum state $J = \ell \pm 1/2$, and isotopic spin state $T = 1/2$.

$\eta_\ell^{\pm}$ = inelastic parameter (defined in Sec. V-1) corresponding to the above phase shift.

$\alpha_\ell^{\pm}$ = phase shift for orbital-angular-momentum quantum number ℓ, total - angular-momentum state $J = \ell \pm 1/2$, isotopic spin state $T = 3/2$.

$\rho_\ell^{\pm}$ = inelastic parameter corresponding to the above phase shift.

For the three reactions in Sec. V.A.2 we have:

Reaction 1, $\pi^+ + p \rightarrow \pi^+ + p$:

$$g(\theta) = -\frac{\lambda n}{2\sin^2\theta/2}\exp[-in\,\ell n(\sin^2(\theta/2))] + \lambda\sum_{\ell=0}^{\ell_{max}}\left[(\ell+1)\frac{\rho_\ell^{+}\exp[2i\,\alpha_\ell^{+}(+)] - \exp[2i\bar{\Phi}_\ell]}{2i} + \ell\,\frac{\rho_\ell^{-}\exp[2i\,\alpha_\ell^{-}(+)] - \exp[2i\bar{\Phi}_\ell]}{2i}\right]P_\ell(\cos\theta), \tag{A.1}$$

$$h(\theta)=\frac{i\lambda n\, B \sin\theta}{2\sin^2\theta/2}+\lambda\sum_{\ell=1}^{\ell_{max}}\left[\frac{\rho_\ell^{+}\exp[2i\alpha_\ell^{+}(+)]-\rho_\ell^{-}\exp[2i\alpha_\ell^{-}(+)]}{2}\right.$$

$$\left.-i\,n\,B\left(\frac{2\ell+1}{\ell(\ell+1)}\right)\right]P_\ell^{1}(\cos\theta); \qquad (A.2)$$

<u>Reaction 2, $\pi^- + p \rightarrow \pi^- + p$:</u>

$$g(\theta)=\frac{\lambda n}{2\sin^2\theta/2}\exp\left\{i\,n\,\ell n(\sin^2\theta/2)\right\}+\lambda\sum_{\ell=0}^{\ell_{max}}\left[(\ell+1)\frac{\rho_\ell^{+}\exp[2i\alpha_\ell^{+}(-)+2\eta_\ell\exp[2i\delta_\ell^{+}(-)]}{6i}\right.$$

$$\left.+\ \ell\frac{\rho_\ell^{-}\exp[2i\alpha_\ell^{-}(-)+2\eta_\ell^{-}\exp[2i\delta_\ell^{-}(-)]}{6i}-(2\ell+1)\frac{\exp[-2i\phi_\ell]}{2i}\right]P_\ell(\cos\theta) \quad (A.3)$$

$$h(\theta)=\frac{i\lambda n\, B\sin\theta}{2\sin^2\theta/2}$$

$$+\sum_{\ell=1}^{\ell_{max}}\left[\frac{\rho_\ell^{+}\exp[2i\alpha_\ell^{+}(-)]+2\eta_\ell^{+}\exp[2i\delta_\ell^{+}(-)-\rho_\ell^{+}\exp[2i\alpha_\ell^{-}(-)-\exp[2i\delta_\ell^{-}(-)]}{6}\right.$$

$$\left.+\,i\,n\,B\left(\frac{2\ell+1}{\ell(\ell+1)}\right)\right]P_\ell^{1}(\cos\theta) \qquad (A.4)$$

<u>Reaction 3, $\pi^- + p \rightarrow \pi^0 + n$</u>

In this reaction, the incoming particles are charged and the outgoing particles are neutral. One may, therefore, to the accuracy desired in this analysis, consider the Coulomb perturbation to be half as great as in reaction 2. Hence when the proper isotopic spin decomposition is used the scattering amplitudes are given by

$$g(\theta) = \frac{\sqrt{2}}{3}\lambda\!\!\!^{-} \sum_{\ell=0}^{\ell_{max}} \left[(\ell+1) \frac{\rho_\ell^+ \exp[2i\alpha_\ell^+(0) - \eta_\ell^+ \exp[2i\delta_\ell^+(0)]}{2i} \right.$$

$$\left. + \ell \frac{\rho_\ell^- \exp[2i\alpha_\ell^-(0)] - \eta_\ell^- \exp[2i\alpha_\ell^-(0)]}{2i} \right] P_\ell(\cos\theta) \qquad (A.5)$$

and

$$h(\theta) = \frac{\sqrt{2}}{3}\lambda\!\!\!^{-} \sum_{\ell=1}^{\ell_{max}} \left[\frac{\rho_\ell^+ \exp[2i\alpha_\ell^+(0)] - \eta_\ell^+ \exp[2i\delta_\ell^+(0)] - \rho_\ell^- \exp[2i\alpha_\ell^-(0)] + \eta_\ell^- \exp[2i\delta_\ell^-(0)]}{2} \right]$$

$$\times P_\ell^1(\cos\theta) \qquad (A.6)$$

The new quantities introduced in Eqs. (A.1) through (A.6) are

$$n = \frac{e^2}{hv}, \qquad (A.7)$$

where v is the lab velocity of the incident pion, and

$$B = \frac{(\mu_P \beta_P \beta_\pi)/2 + 4(2\mu_P - 1)\beta_P^2/4}{1 + \beta_\pi \beta_P}, \qquad (A.8)$$

where μ_P = magnetic moment of the proton in nuclear magnetons, and β_P, β_π = c.m. velocities of the proton and pion divided by the velocity of light.

The Φ_ℓ is the nonrelativistic Coulomb phase shift of order ℓ. It is equal to 0 for $\ell = 0$, and is given by

$$\Phi_\ell = \sum_{x=1}^{\ell} \tan^{-1}\left(\frac{n}{x}\right), \quad \text{for } \ell \geq 1. \qquad (A.9)$$

The additional symbols(+, -or 0) that appear on the phase shifts in Eqs. (A.1) through (A.6) are necessary because the phase shifts used in those expressions are total phase shifts, differing from the nuclear shifts by a small term $\Phi_\ell^{\pm}$, which is the complete Coulomb phase shift of order ℓ. This is explained below. The total phase shifts are related to the nuclear shifts by

$$a_\ell^{\pm}(+) = a_\ell^{\pm} + \Phi_\ell^{\pm} ,$$
$$a_\ell^{\pm}(-) = a_\ell^{\pm} - \Phi_\ell^{\pm}$$

and

$$\delta_\ell^{\pm}(-) = \delta_\ell^{\pm} - \Phi_\ell^{\pm}$$
$$a_\ell^{\pm}(0) = a_\ell^{\pm} - \Phi_{\ell/2}^{\pm}$$
$$\delta_\ell^{\pm}(0) = \delta_\ell^{\pm} - \Phi_{\ell/2}^{\pm}$$

The complete Coulomb phase shift of order ℓ, $\Phi_\ell^{\pm}$ consists of the nonrelativistic Coulomb phase shift defined by Eq. (A.9), plus a first-order nonrelativistic correction,

$$\Phi_\ell^{\pm} = \Phi_\ell + \Delta\Phi_\ell^{\pm} , \tag{A.10}$$

where the first-order nonrelativistic Coulomb term is given by

$$\Delta\Phi_0 \approx n[(1/2)(\beta_P\beta_\pi) + (1/4)(2\mu_P - 1)\,\beta_P^2/(1 + \beta_\pi\,\beta_P)], \tag{A.11}$$

$$\Delta\Phi_\ell^{+} \approx n\,B/(\ell + 1), \qquad \text{for } \ell \geqslant 1, \tag{A.12}$$

and

$$\Delta\Phi_\ell^{-} \approx -\frac{nB}{\ell}, \quad \text{for } \ell \geqslant 1. \tag{A.13}$$

All quantities used in Eqs. (A.11) through (A.13) are defined in conjunction with Eqs. (A.7) and (A.8).

The above Coulomb phase shifts for incident-pion kinetic energy T_π = 310 MeV are given in Table A I.

Table AI. Nonrelativistic Coulomb phase shifts, first-order relativistic corrections, and complete Coulomb phase shift (all in deg) for incident-pion kinetic energy $T_\pi = 310$ MeV.

ℓ	Φ_ℓ	$\Delta\Phi_\ell^+$	$\Delta\Phi_\ell^-$	Φ_ℓ^+	Φ_ℓ^-
0	0.00	0.09	----	0.09	----
1	0.44	0.09	-0.17	0.53	0.27
2	0.66	0.06	-0.09	0.72	0.57
3	0.81	0.04	-0.06	0.95	0.75

Appendix B. Tables of Error Matrices for spd and spdf Solutions

Table BI. Error matrix for spd solution (expressed in deg^2).

	$S_{3,1}$	$P_{3,1}$	$P_{3,3}$	$D_{3,3}$	$D_{3,5}$	$S_{1,1}$	$P_{1,1}$	$P_{1,3}$	$D_{1,3}$	$D_{1,5}$
$S_{3,1}$	0.4	0.2	0.2	0.1	-0.2	-0.2	-0.2	-0.0	-0.1	0.1
$P_{3,1}$		0.3	0.1	0.1	-0.2	-0.1	-0.2	-0.0	-0.0	0.1
$P_{3,3}$			0.4	0.0	0.0	0.0	-0.1	0.2	-0.1	0.2
$D_{3,3}$				0.1	-0.1	-0.1	-0.0	-0.0	-0.0	0.0
$D_{3,5}$					0.2	0.1	0.1	0.1	0.0	-0.0
$S_{1,1}$						0.4	0.0	0.5	0.0	0.1
$P_{1,1}$							0.2	-0.1	0.1	-0.2
$P_{1,3}$								0.8	-0.1	0.3
$D_{1,3}$									0.1	-0.1
$D_{1,5}$										0.4

Table BII. Error matrix for spdf solution I (expressed in deg^2).

	$S_{3,1}$	$P_{3,1}$	$P_{3,3}$	$D_{3,3}$	$D_{3,5}$	$F_{3,5}$	$F_{3,7}$	$S_{1,1}$	$P_{1,1}$	$P_{1,3}$	$D_{1,3}$	$D_{1,5}$	$F_{1,5}$	$F_{1,7}$
$S_{3,1}$	3.2	3.3	0.5	1.5	-1.7	-0.0	-0.9	-1.5	-1.3	-1.5	-0.2	-0.1	0.0	0.7
$P_{3,1}$		3.8	0.4	1.8	-1.9	-0.0	-1.1	-1.7	-1.4	-1.7	-0.2	-0.3	0.1	0.8
$P_{3,3}$			0.4	0.1	-0.1	0.0	-0.1	-0.2	-0.3	-0.0	-0.1	0.2	0.0	0.1
$D_{3,3}$				0.9	-0.9	0.0	-0.5	-0.8	-0.6	-0.8	-0.1	0.2	0.0	0.3
$D_{3,5}$					1.0	0.0	0.5	0.9	0.7	0.9	0.1	0.2	-0.0	-0.4
$F_{3,5}$						0.1	-0.0	-0.0	-0.0	-0.0	-0.0	-0.0	-0.0	-0.0
$F_{3,7}$							0.3	0.5	0.4	0.5	0.1	0.1	-0.0	-0.2
$S_{1,1}$								2.2	0.6	1.3	0.3	0.5	-0.2	0.3
$P_{1,1}$									0.7	0.5	0.2	-0.1	0.0	-0.3
$P_{1,3}$										1.7	-0.0	0.6	-0.0	-0.3
$D_{1,3}$											0.1	-0.1	-0.0	0.1
$D_{1,5}$												0.6	-0.0	0.1
$F_{1,5}$													0.1	-0.1
$F_{1,7}$														0.5

Table BIII. Error matrix for spdf solution II (expressed in deg^2).

	$S_{3,1}$	$P_{3,1}$	$P_{3,3}$	$D_{3,3}$	$D_{3,5}$	$F_{3,5}$	$F_{3,7}$	$S_{1,1}$	$P_{1,1}$	$P_{1,3}$	$D_{1,3}$	$D_{1,5}$	$F_{1,5}$	$F_{1,7}$
$S_{3,1}$	0.2	0.1	0.1	0.1	-0.1	0.0	-0.0	0.2	0.1	0.0	0.0	0.0	-0.0	-0.0
$P_{3,1}$		0.7	-0.4	0.5	-0.6	0.3	-0.3	0.2	-0.2	0.2	-0.2	0.3	-0.1	0.1
$P_{3,3}$			0.7	-0.3	0.5	-0.2	0.2	0.2	0.4	-0.1	0.2	-0.2	0.1	-0.1
$D_{3,3}$				0.4	-0.4	0.2	-0.2	0.1	-0.1	0.1	-0.2	0.2	-0.1	0.1
$D_{3,5}$					0.6	-0.2	0.3	-0.1	0.1	-0.1	0.2	-0.3	0.1	-0.1
$F_{3,5}$						0.2	-0.1	0.1	-0.1	0.1	-0.1	0.1	-0.1	0.1
$F_{3,7}$							0.2	-0.1	0.1	-0.1	0.1	-0.1	0.1	-0.1
$S_{1,1}$								1.8	0.7	0.4	0.1	0.1	-0.1	0.1
$P_{1,1}$									0.9	0.1	0.3	0.1	0.1	-0.0
$P_{1,3}$										0.5	0.0	0.2	-0.0	0.1
$D_{1,3}$											0.2	-0.0	0.1	-0.0
$D_{1,5}$												0.3	-0.2	0.1
$F_{1,5}$													0.1	-0.1
$F_{1,7}$														0.1

Table BIV. Error matrix for spdf solution III (expressed in deg^2).

	$S_{3,1}$	$P_{3,1}$	$P_{3,3}$	$D_{3,3}$	$D_{3,5}$	$F_{3,5}$	$F_{3,7}$	$S_{1,1}$	$P_{1,1}$	$P_{1,3}$	$D_{1,3}$	$D_{1,5}$	$F_{1,5}$	$F_{1,7}$
$S_{3,1}$	1.9	2.2	0.2	1.2	-1.1	0.2	-0.7	0.4	-0.7	0.8	-0.6	0.6	-0.1	0.4
$P_{3,1}$		3.0	0.1	1.7	-1.4	0.2	-0.9	0.4	-1.1	1.1	-0.8	0.7	-0.1	0.6
$P_{3,3}$			0.4	0.0	0.0	0.0	-0.0	0.2	0.3	0.2	-0.0	0.0	0.0	0.0
$D_{3,3}$				1.1	-0.8	0.1	-0.6	0.2	-0.7	0.6	-0.5	0.4	-0.1	0.3
$D_{3,5}$					0.8	-0.1	0.4	-0.2	0.6	-0.5	0.4	-0.4	0.1	-0.3
$F_{3,5}$						0.1	-0.1	0.0	-0.1	0.1	0.1	0.0	-0.0	0.0
$F_{3,7}$							0.3	-0.1	0.4	-0.3	0.2	-0.2	0.0	-0.2
$S_{1,1}$								1.9	0.2	1.0	-0.7	0.4	-0.4	0.0
$P_{1,1}$									1.6	-0.6	0.4	-0.3	0.2	-0.2
$P_{1,3}$										1.0	-0.5	0.5	-0.3	0.2
$D_{1,3}$											0.6	-0.2	0.1	-0.1
$D_{1,5}$												0.3	-0.1	0.2
$F_{1,5}$													0.2	0.0
$F_{1,7}$														0.1

REFERENCES

1. E. H. Rogers, O. Chamberlain, J. Foote, H. Steiner, C. Wiegand, and T. Ypsilantis, Revs. Modern Phys. 33, 356 (1961).
2. J. H. Foote, O. Chamberlain, E. Rogers, H. Steiner, C. Wiegand, and T. Ypsilantis, Phys. Rev. 122, 948 (1961).
3. J. H. Foote, O. Chamberlain, E. Rogers, and H. Steiner, Phys. Rev. 122, 959 (1961).
4. Olav T. Vik (Lawrence Radiation Laboratory), private communication.
5. John C. Caris, Charge-Exchange Scattering of Negative Pions by Hydrogen at 230, 260, 290, 317, and 371 MeV, Lawrence Radiation Laboratory Report UCRL-9048, March 1960 (unpublished).
6. V. Zinov and S. Korenchenko, Soviet Phys.-JETP 11, 794 (1960).
7. I. M. Vailevskii and V. V. Vishnyakov, Soviet Phys.—JETP 11, 323 (1960).
8. O. Chamberlain, E. Segre, and C. Wiegand, Phys. Rev. 83, 923 (1951).
9. J. H. Atkinson and V. Perez-Mendez, Rev. Sci. Instr. 30, 865 (1959).
10. R. L. Garwin, Rev. Sci. Instr. 21, 569 (1950).
11. J. Mey, 10-Mc Pulse Amplitude Discriminator, Lawrence Radiation Laboratory Report UCRL-3307 Rev., Jan. 1959, Sec. CC3, p. 8.
12. R. H. Dalitz, Proc. Phys. Soc. (London) A64, 667 (1951).
13. William A. Wenzel, Millimicrosecond Coincidence Circuit for High-Speed Counting, University of California Radiation Laboratory Report UCRL-8000, October 1957 (unpublished).
14. V. Zinov and S. Korenchenko, Soviet Phys.-JETP 11, 1010 (1960).
15. John H. Atkinson, Jr. and Beverly Hill Willis, High-Energy Particle Data, Lawrence Radiation Laboratory Report UCRL-2426-June 1957 (unpublished), Vol. II, p. 65.
16. A. Borsellino, Phys. Rev. 89, 1023 (1953).

17. W. Heitler, Quantum Theory of Radiation, 3rd Edition (Oxford University Press, London, 1954), p. 256 ff.
18. D. Josephs, Nuovo cimento 16, 997 (1960).
19. M. Derrick, J. Fetkovich, T. Fields, and J. Deahl, Phys. Rev. 120, 1022 (1960).
20. R. M. Sternheimer, Phys. Rev. 101, 384 (1956).
21. R. M. Sternheimer, Rev. Sci. Instr. 25, 1070 (1954).
22. D. B. Chelton and D. B. Mann, Cryogenic Data Book, University of California Radiation Laboratory Report UCRL-3421, May 1956 (unpublished).
23. V. G. Zinov, A. D. Konin, S. M. Korenchenko, and B. Pontecorvo, Soviet Phys.-JETP 11, 1233 (1960).
24. J. Ashkin, Nuovo cimento Suppl. 14 Ser. X, No. 2, 221 (1959).
25. H. A. Bethe and F. de Hoffmann, Mesons and Fields, (Row, Peterson and Company, Evanston, Illinois, 1955), Vol. II, p. 60.
26. E. Fermi, N. Metropolis, and E. F. Alei, Phys. Rev. 95, 1581 (1954).
27. H. L. Anderson, W. C. Davidon, M. Glicksman, and U. E. Kruse, Phys. Rev. 100, 279 (1955).
28. H. L. Anderson and W. C. Davidon, Nuovo cimento 5, 1238 (1957).
29. C. Thompson, Biometrika 32, 188 (1941).
30. William J. Willis, Phys. Rev. 116, 753 (1959).
31. L. S. Rodberg, Phys. Rev. Letters 3, 58 (1959).
32. Walton A. Perkins, III, Positive Pion Production by Negative Pions (thesis) Lawrence Radiation Laboratory Report UCRL-8778, June, 1959.
33. B. C. Barish, J. Solomon, and R. Kurz (Lawrence Radiation Laboratory), private communication.
34. M. MacGregor, M. Moravcsik, and H. P. Noyes, Phys. Rev. 123, 1835 (1961).
35. G. F. Chew, M. Goldberger, F. Low, and Y. Nambu, Phys. Rev. 106, 1337 (1957).

36. T. D. Spearman, Nuovo cimento 15, 147 (1960).

37. H. P. Stapp, T. J. Ypsilantis, and N. Metropolis, Phys. Rev. 105, 302 (1957).

38. Frank T. Solmitz, Phys. Rev. 94, 1799 (1954).

39. C. L. Critchfield and D. C. Dodder, Phys. Rev. 76, 602 (1949).

This report was prepared as an account of Government sponsored work. Neither the United States, nor the Commission, nor any person acting on behalf of the Commission:

A. Makes any warranty or representation, expressed or implied, with respect to the accuracy, completeness, or usefulness of the information contained in this report, or that the use of any information, apparatus, method, or process disclosed in this report may not infringe privately owned rights; or

B. Assumes any liabilities with respect to the use of, or for damages resulting from the use of any information, apparatus, method, or process disclosed in this report.

As used in the above, "person acting on behalf of the Commission" includes any employee or contractor of the Commission, or employee of such contractor, to the extent that such employee or contractor of the Commission, or employee of such contractor prepares, disseminates, or provides access to, any information pursuant to his employment or contract with the Commission, or his employment with such contractor.